

INVESTIGATION OF A LOW HEAT LOSS HIGH
TEMPERATURE THERMAL ENERGY STORAGE SYSTEM

BY

NORMAN ALAN COPE

A DISSERTATION PRESENTED TO THE GRADUATE COUNCIL
OF THE UNIVERSITY OF FLORIDA IN PARTIAL
FULFILLMENT OF THE REQUIREMENTS FOR THE DEGREE
OF DOCTOR OF PHILOSOPHY

UNIVERSITY OF FLORIDA

1981

Copyright 1981

by

Norman Alan Cope

ACKNOWLEDGEMENTS

I would like to express my deepest gratitude to Dr. Erich A. Farber, for his inspiring guidance and encouragement during my course of this research. I would also like to express my thanks to the other members of my committee for their constructive criticism and advice during the course of this work.

I would like to acknowledge the helpful assistance of the Shop personnel ably led by Mr. Richard Tomlinson.

I would like to acknowledge the patience and encouragement of my wife, Elizabeth, without whose help this work would not have been possible.

Finally, I would like to thank my typist, Denise Jobb, for her excellent typing and assistance in preparing this dissertation and John Murdoch for his assistance in preparing some of the drawings of this text.

TABLE OF CONTENTS

	Page
ACKNOWLEDGEMENTS	iii
LIST OF TABLES	vii
LIST OF FIGURES	viii
LIST OF SYMBOLS	x
ABSTRACT	xiv
CHAPTER	
I INTRODUCTION	1
II LITERATURE REVIEW	10
III THEORETICAL CONSIDERATIONS OF POWDER INSULATION	17
Introduction	17
Theoretical Model	18
Thermal Conductivity of a Perfect Gas	21
Thermal Conductivity of a Non-Continuum Gas	25
Particle-to-Particle Conductivity of a Porous Powder	32
Radiant Transfer in a Porous Medium	44
IV EQUIPMENT DESIGN AND MATERIAL PREPARATION	
Introduction	49
Conductivity Test Apparatus	49
The Design of High Temperature Thermal Energy Storage System	56
Diatomaceous Earth Properties	64

	Page
V EXPERIMENTAL PROCEDURE AND RESULTS	73
Conductivity Test Equipment	73
Thermal Conductivity of Powder Insulation Under Vacuum	76
Data and Results from Thermal Conductivity Test	77
Discussion of Results of Conductivity Test	78
Range of values	78
Radiative transfer	81
Effective gas conductivity	82
Particle-to-particle conductivity ...	86
Effect of particle size in a non- continuum	97
Effect of a vacuum level	98
Effect of carbon and iron in diatomaceous earth	100
Thermal Energy Storage System	101
Results of Prototype Thermal Energy Storage System Test	105
Discussion of Results for the Thermal Energy Storage System Test	108
Insulation performance	108
Heating of organic oil	111
Steel wool blanket	112
Overall storage vessel performance ..	112
Tank support	114
Cost of high temperature storage	114
Uncertainty in the measurement of K_a	117
VI CONCLUSIONS AND RECOMMENDATIONS	118
APPENDIX A - STORAGE VESSEL TEST DATA	122
APPENDIX B - CONVECTION HEAT TRANSFER ANALYSIS FOR A POROUS POWDER	130
APPENDIX C - UNCERTAINTY IN THE MEASUREMENT OF K_a	135
BIBLIOGRAPHY	140

	Page
EXTENDED BIBLIOGRAPHY	143
BIOGRAPHICAL SKETCH	144

LIST OF TABLES

Table		Page
1	High Temperature Insulators	16
2	Molecular Weight, Collision Diameter, and Specific Heat Ratio of Selected Gases	24
3	Diatomaceous Earth Particle Size and Distri- bution - Typical Results	67
4	Particle Density and Void Fraction of Diatomaceous Earth	71
5	Average Thermal Conductivity Values For Evacuated Diatomaceous Earth	79
6	Theoretical Thermal Conductivity of Air and Argon For Non-Continuum Conditions at $T_b = 860^\circ R$	84
7	Proportioning of Thermal Conductivity into Gaseous and Solid-to-Solid Conductivity	87
8	Estimated Manufacturer's Cost for Storage Vessels	116

LIST OF FIGURES

Figure		Page
1	Schematic of a Residential Energy System Using High Temperature Thermal Energy Storage	6
2	Mechanistic Description of Heat Transfer Through Porous Powder	19
3	Idealization of a Contact Region	34
4	Two Particles Forming A Contact Region	39
5	Model for Derivation of Radiant Contribution to Thermal Conductivity Through a Porous Medium	45
6	Conductivity Test Apparatus	50
7	Prototype High Temperature Thermal Energy Storage System	57
8	Electron Microscope Photograph of Diatomaceous Earth - Carbon (1% wt.) Mixture. Particles from Tyler Sieve #500	68
9	Electron Microscope Photograph of Diatomaceous Earth - Carbon (1% wt.) Mixture. Particles from Tyler Sieve #170	68
10	Electron Microscope Photograph of Diatomaceous Earth (as purchased)	69
11	Electron Microscope Photograph of Carbon Black (Monarch 500)	69
12	Conductivity Test Equipment Arrangement	74
13	Conductivity Test Equipment	75
14	Electron Microscope Photograph of Surface of Diatomaceous Earth Particle, Tyler Sieve #500	92

Figure		Page
15	Electron Microscope Photograph of Surface of Diatomaceous Earth Particle, Tyler Sieve #170	92
16	Apparent Thermal Conductivity of Selected Diatomaceous Earth - Carbon (1% wt.) Particles	96
17	Gas Conduction vs. Gas Pressure in Powders Under Vacuum (Theoretical)	99
18	Thermocouple Location for Prototype High Temperature Thermal Energy Storage Vessel	103
19	Cool-Down of Prototype High Temperature Thermal Energy Storage System	106
20	Temperature Profile Through Powder Insula- tion Under Vacuum	107
21	Storage System Test Equipment Arrangement	109

LIST OF SYMBOLS

A	area, ft ²
A _a	aperture area, ft ²
A _{gc}	gas conduction area, ft ²
A _s	solid conduction area, ft ²
A _T	total area, ft ²
A _n	Avogadro's number
a	accommodation coefficient (dimensionless)
\bar{a}	average accommodation coefficient (dimensionless)
B	variable, lb _f /ft
b	length, ft
Btu	British Thermal Unit
C	correction factor (dimensionless)
\bar{C}	average molecular velocity, ft/sec.
C'	correction factor, contact points/particle
C _p	specific heat at constant pressure, Btu/lb _m °F
C _v	specific heat at constant volume, Btu/lb _m °F
D	diameter, ft
\bar{d}	mean void diameter, ft
D _c	equivalent contact diameter, ft
D _n	nominal particle diameter, ft
dx	differential length, ft
e	correction factor, dimensionless
E	Young's modulus, psi
F	force, lb _f
°F	degree Fahrenheit
ft	feet
ft ²	square feet
ft ³	cubic feet
G	constant, dimensionless

h	convective heat transfer coefficient, Btu/hrft ² °F
H_{in}	rate of energy input, Btu/hr
hr	hour
H_{sto}	rate of energy storage, Btu/hr
I	current, A
I_s	insolation, Btu/hrft ²
in.	inch
K	thermal conductivity, Btu/hrft° F
K_a	apparent thermal conductivity, Btu/hrft° F
k_f	thermal conductivity of a fluid, Btu/hrft° F
K_g	thermal conductivity coefficient of a gas for continuum, Btu/hrft° F
\bar{K}_g	thermal conductivity coefficient of a gas for continuum, transition, and non-continuum, Btu/hrft° F
Kn	Knudsen number, λ/\bar{d} , dimensionless
K_r	radiative conductivity coefficient, Btu/hrft° F
k_{rv}	radiative transfer through particle voids, Btu/hrft° F
K_s	thermal conductivity coefficient through a particle bed, Btu/hrft° F
\bar{K}_s	modified thermal conductivity coefficient through a particle bed, Btu/hrft° F
k_s	thermal conductivity of a particle, Btu/hrft° F
L	modified mean free path or length, ft
lb_m	pounds mass
lb_f	pounds force
M	molecular weight, lb_m/lb_m -mole
mm Hg	millimeters of mercury
min	minute
n	contact regions per particle
N_A	particles per unit area
N_h	particles per unit length
Nu	Nusselt number, dimensionless

OD	outside diameter, ft
P	pressure, lb_f/ft^2
psi	pressure difference, lb_f/in^2
psig	gauge pressure, lb_f/in^2
Q	heat transfer, Btu/hr
Q'''	energy generated per unit volume, Btu/hrft^3
q_c	heat transfer by convection, Btu/hrft^2
Q_{elec}	electrical energy dissipation, Btu/hr
q_{gc}	heat transfer by gas conduction, Btu/hrft^2
q_h	heat transfer by convection, Btu/hrft^2
Q_{loss}	heat loss, Btu/hr
q_r	radiation transfer, Btu/hrft^2
q_s	heat transfer through solids, Btu/hrft^2
Q_T	heat transfer, Btu/hr
q_T	heat flux, Btu/hrft^2
R_e	resistance to heat flow, $\text{hrft}^\circ\text{F/Btu}$
R	particle radius, ft
$^\circ\text{R}$	degree Rankine
r	radial coordinate, ft
r_i	inner tank radius, ft
r_o	outer tank radius, ft
R_u	universal gas constant, $1.986 \text{ Btu/lb}_m\text{-mole } ^\circ\text{R}$
S	average stress, lb_f/in^2
T	temperature, $^\circ\text{F}$, $^\circ\text{R}$
T_b	average or bulk powder temperature, $^\circ\text{F}$, $^\circ\text{R}$
T_C	average temperature of hot boundary surface, $^\circ\text{F}$
T_H	average temperature of cold boundary surface, $^\circ\text{F}$
T_o	average surface temperature, $^\circ\text{F}$, $^\circ\text{R}$
V	volume, ft^3
wt	weight, lb_f
x	length or X-axis coordinate
y	particle contact radius, ft
z	coordinate direction, ft

GREEK SYMBOLS

α	thermal diffusivity, ft^2/hr
β	constant, dimensionless
γ	specific heat ratio, dimensionless
δ	void fraction, dimensionless
Δ	finite change of variable
ϵ	emissivity, dimensionless
ξ	Stephan-Boltzmann constant, 0.1714×10^{-8} $\text{Btu/hr ft}^2\text{ }^\circ\text{R}^4$
η_τ	thermal efficiency, dimensionless
θ	coordinate direction, degrees
λ	mean free path in a continuum, ft
μ	Poisson ratio, dimensionless
μ_f	viscosity, lbm/hrft
$\mu\text{m Hg}$	micrometers of mercury
ρ	density lb_m/ft^3
σ	collision diameter, ft
τ	time, hours
ϕ	phase angle

Abstract of Dissertation Presented to the Graduate
Council of the University of Florida in Partial
Fulfillment of the Requirements for the Degree
of Doctor of Philosophy

INVESTIGATION OF A LOW HEAT LOSS HIGH
TEMPERATURE THERMAL ENERGY STORAGE VESSEL

By

Norman Alan Cope

May 1982

Chairman: Erich A. Farber
Major Department: Mechanical Engineering

A low heat loss thermal energy storage system capable of storage in a range of 250-1000°F is described in this dissertation. The design criteria called for a storage system that would be simple to construct, use inexpensive and readily available materials, utilize an insulating material with a thermal conductivity between 0.003 - 0.015 Btu/hrft°F for temperatures ranging between 250-1000°F, and be suitable for residential or commercial applications.

A design selected to fulfill the above criteria consists of a double tank wherein the annular space between the tanks is filled with a porous powder (silica) and then evacuated to a pressure of approximately 1 mm Hg. Thermal conductivity values of 0.0029 - 0.110 Btu/hrft°F were achieved experimentally for vacuum levels ranging from 0.5 - 3.0 mm Hg and hot surface temperatures ranging from 340 - 711°F.

The results of an analysis of the modes of heat transfer through the porous powder under vacuum indicate several means of potential improvement in the conductivity of an insulating powder. Based on theoretical considerations, the means for reducing the conductivity include

1. selecting powder materials with a low thermal conductivity, such as quartz particles,
2. selecting a particle size where an average void dimension is obtained that is less than or equal to the mean free path of the gas molecules at a selected operating condition,
3. selecting gases whose properties inhibit free-molecular energy transport, such as gases with high molecular weights, high specific heat ratios and large molecular cross-sections; several of the more practical gases being air, argon and carbon dioxide.

The results of this study indicate for the temperature range investigated, 250-1000°F, thermal energy storage is technically and economically feasible. The availability of inexpensive thermal energy storage will make it possible to use current energy resources more effectively, particularly those that occur on an intermittent basis, such as direct solar (thermal). The concept of thermal energy storage in the temperature range indicated suggests the possibility of an independent energy system, particularly for residential and commercial applications.

CHAPTER I

INTRODUCTION

The more successful techniques used to store energy, electrical or thermal, involve chemical or mechanical techniques such as lead-acid batteries and thermal energy storage, respectively. There has been little practical advancement in energy storage technology over the techniques just mentioned. With the current emphasis on energy efficiency, there is a need to examine the benefits of developing and using energy storage devices. In many applications the need for thermal energy is greater than the need for electrical energy. For example, in a household, about 85% of the energy needs can be provided by thermal energy. This quantity of thermal energy is needed for house heating, house cooling by absorption air-conditioning,^{*} domestic water heating, and cooking. The remaining 15% of the energy requirements, for current lifestyles, is needed in the form of electricity for lighting, refrigeration and powering communications systems, fans and pumps.

* It should be noted that a gas-fired or hot water driven absorption air conditioner generally requires electricity to run pumps and controls.

It should be recognized in the above example that energy, in the form of either heat or work, is most effective when used in a direct manner. For example, when thermal energy is converted into electrical energy (work), there follows a substantial loss as a result of the second law of thermodynamics in the form of the Carnot principle. And while electric energy (work) can be converted into thermal energy with no loss, the Carnot loss suffered in creating work from heat can be substantial. However, from a systems point of view, one may wish to convert from one form of energy to another for convenience, to enhance the system usefulness, or to enhance the life-cycle cost of the system.

Research and development of materials for storing thermal energy indicate that energy storage on a residential, commercial and industrial scale is feasible. Phase change materials, such as nitrate salts, can store large quantities of latent thermal energy associated with its phase change and organic oils, such as cottonseed oil, can be used to store large quantities of sensible thermal energy.

A primary difficulty of storing thermal energy at temperatures of 250-1000°F is that one must find an economical means of constructing a storage system with low heat loss characteristics. Very little literature exists in this area. Most of the research efforts in the past have been limited to developing insulation and insulating techniques in the cryogenic field.

Many of the problems encountered in insulating a cryogenic vessel are also encountered in insulating a high temperature system. Therefore, the cryogenic area seems to be a good starting point for developing a high temperature thermal energy storage system. Shared problems in the development of high temperature or cryogenic storage container are

- 1) heat leaks due to supports and tank penetrations,
- 2) insulation and tank materials,
- 3) outgassing of materials in the evacuated space,
- 4) inner tank support structure,
- 5) leak-free penetration ports for piping and electrical wiring,
- 6) improved evacuating techniques when fine powders are used as the insulating material, and
- 7) reasonable material and system cost.

The solutions to the above problems are different for cryogenic than for high temperature. For example, in cryogenic vessels, some plastics can be utilized as a spacing material; whereas, this same material in moderate or high temperature environments would cause problems like loss of structural integrity or outgassing.

In constructing a high temperature storage vessel there are different concepts that one may employ to achieve the same results. For example, one could build a storage vessel using a fibrous insulating material under a vacuum

but, obviously, this material would not support the inner vessel. A porous powder under vacuum could be used to support the inner vessel and to insulate the inner tank as well. Both insulating materials may result in a similar heat loss characteristic; however, there may be advantages and disadvantages with using one material in place of the other.

This study investigated the use of powder insulation at a typical pressure level of 1 mm Hg for insulating a high temperature thermal energy storage system. This technique of insulating was chosen over multi-layer insulation because

- 1) powder insulation works well at pressures of 1-10 mm Hg and this level is easier to maintain than a pressure level of 1 μ m Hg or less, as required by multi-layer insulation,
- 2) suitable powders for withstanding high temperatures are readily available,
- 3) a need exists for many uses in high temperature technology,
- 4) it may be possible to form a load bearing member of powder to support the inner vessel and this would avoid the structural complexities of building thick walled vessels.

Powder insulations suitable for high temperatures are readily available and can be anything from wood ash to sand. The particular material used in this study was diatomaceous earth, a material readily available, inexpensive, and suitable for high temperature use because of low

particle thermal conductivity and a softening point* of 1600°F.

Projected applications of high temperature storage systems.

The intention of developing a high temperature thermal energy storage system was to provide this component in a self-contained cooking system for residential use [1]. This system utilizes a concentrating collector with an automatic solar powered tracking mechanism [2], a heat storage vessel, and a cooking range. The concentrating collector coolant and the heat storage media are organic oil.

Four organic oils (cottonseed, peanut, corn and soybean oil) were evaluated for the above use [3]. In operation, the organic oil was heated as it circulated through a heat exchanger located in the focal point of the collector. With a minimum temperature of 400°F, the heated fluid contained in the storage vessel would circulate through the heating coils of the cooking range. The main advantage of this system is that thermal energy is accumulated and stored for use at a later time, eliminating the disadvantage of having to wait for direct radiation and the necessity to cook outdoors.

The system can also be used as the basis for an integrated, residential power system as shown in Figure 1. For

* A softening point represents a temperature beyond which the yield stress of a material drops off rapidly with increasing temperature.

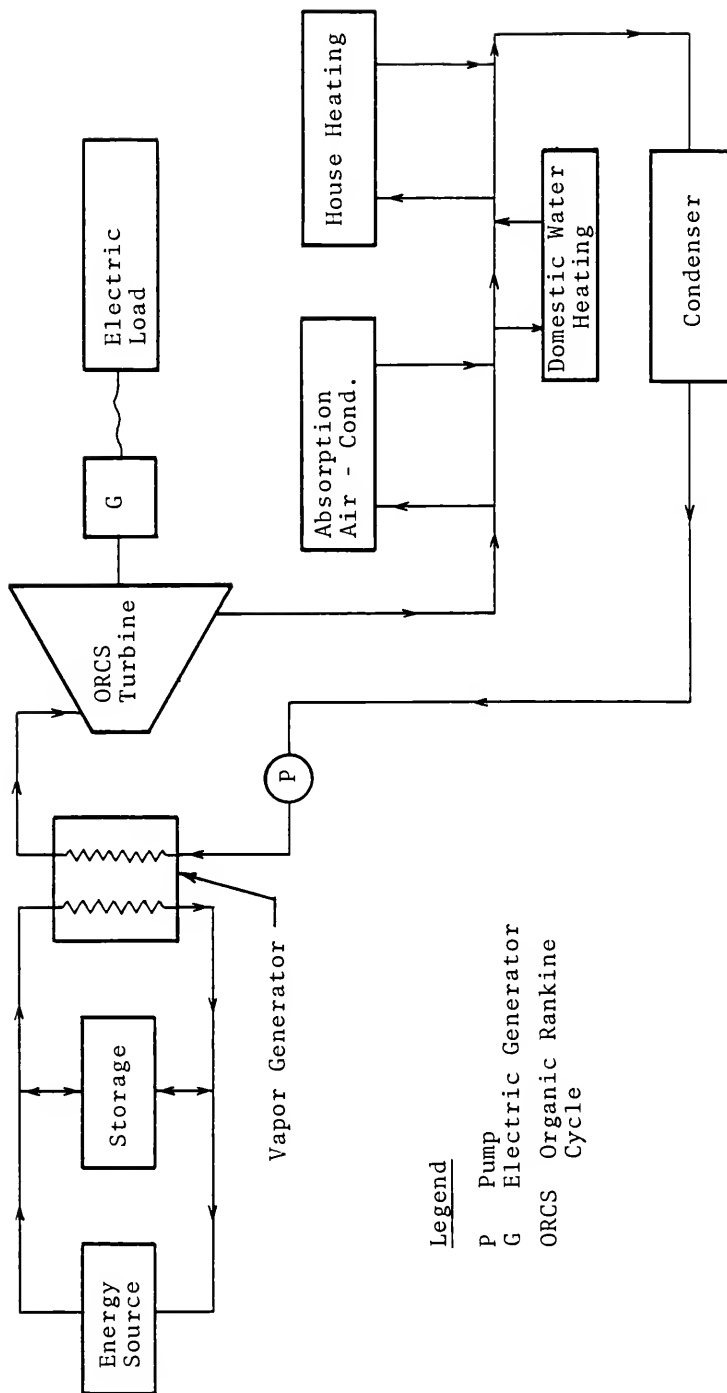


Figure 1

Schematic of a Residential Energy System
Using High Temperature Thermal Energy Storage

example, energy accumulated in the storage vessel can be used to drive a heat engine to produce electricity. The energy rejected from the continuously operating heat engine can be used to drive either an absorption air conditioner or heater, domestic water heater, or similar low temperature devices. The high temperature storage medium, such as organic oil, can be used to power a cooking range.

Energy for the above system may be collected from available energy resources. Some of these possible resources are

- 1) direct solar, thermal conversion,
- 2) fossil or nuclear fuel in the form of off-peak electricity,
- 3) direct solar, electrical to thermal energy conversion (photovoltaic cells),
- 4) wind energy (mechanical to thermal energy conversion).

As emphasized earlier energy is best used in a direct manner; that is, work is best used as work and thermal energy as thermal energy. Processes that convert thermal energy to work, as in the conversion of solar energy to electric in a photovoltaic cell (3) or to wind (4), processes that transform work into thermal energy, such as in statements 3 and 4 above will have irreversible losses associated with them and these losses will be substantial. This concept is embodied in the second law of thermodynamics and may be reviewed in elementary texts on thermodynamics [4]. However, it could nevertheless be economically practical to convert work

into thermal energy. For example, if an industrial process requires high temperature fluids, it might prove advantageous to purchase electrical energy at reduced rates from a utility company during periods of low demand and to convert that power into thermal energy to be stored for later use.

As apparent from the above paragraphs, the listed energy resources occur on an intermittent basis and may not coincide with the energy use pattern for which they were intended. Storing energy for later use transforms an intermittent source of energy into a potentially continuous commodity.

In addition to residential applications an efficient cost effective insulating technique is needed for high temperature batteries [5]. For example, a lithium-sulfur battery operates between 707 - 797°F and a sodium-sulfur battery operates between 446 - 572°F. A particular problem associated with operating these batteries is that energy must be supplied to bring them to operating temperature and to maintain stand-by losses. This energy is not available for work and must be viewed as lost work. If an efficient and cost effective insulating jacket reduced these losses, then high temperature batteries would be one step closer to reality.

Scope of investigation. The goal of this research was to develop a thermal energy storage system suitable for storing latent or sensible thermal energy between temperatures of 250 to 1000°F. The particular objectives required to obtain this goal were to

- 1) find a practical insulating technique capable of reducing the thermal conductivity to less than 0.015 Btu/hrft°F @ 1000°F,
- 2) identify and experimentally determine the necessary thermo-physical properties of the insulating material,
- 3) construct a high temperature thermal energy storage system to verify the thermodynamic analysis and results of the insulating material and to verify the system design.

CHAPTER II

LITERATURE REVIEW

One of the more important facts to emerge from the literature review was that no significant references were found concerning efficient, high temperature insulation suitable for residential or commercial sized thermal energy storage systems. This search included a manual search of the library at the University of Florida and a computer search that included the National Aeronautics and Space Administration (NASA) and the National Technical Information Service (NTIS) engineering files.

In view of the above, the goal of this research was to develop a thermal energy storage system suitable for storing latent or sensible thermal energy between temperatures 250 - 1000°F. The successful development of a thermal energy storage system depends upon the type and quality of the insulation used in constructing the system. The initial literature review shows that there are basically three types of insulation suitable for the indicated temperature range. Based on physical structure they can be described as

- 1) fibrous insulation,
- 2) laminated insulation,
- 3) granular insulation.

Fibrous insulation includes such materials as fiberboard and rockwool, which are suitable for low and moderate temperature applications. Laminated insulation consists of alternating layers of low density insulation such as ceramic paper and low emittance radiation shields. Granular insulation includes such materials as sand, microspheres of glass, and diatomaceous earth. Laminated and granular insulation are suitable for use from cryogenic to high temperature applications.

As described by Jakob [6], some of the earliest work on conduction through porous material was done by such men as Maxwell, Nusselt and Eucker. These investigators included gross simplifications of the heat transfer mechanisms in their analyses. Their aim was to make it possible to obtain reasonable answers to a very complex problem with a minimum of data. It seems that little advancement has been made in the area of heat transfer through porous materials since these early studies.

The basic ideas presented by Reference 6 concerning Maxwell's, Nusselt's, and Eucker's analyses indicate that all three viewed a porous body as either a base material with small particles of another substance distributed throughout that material, or as alternating layers of solids and gases with heat flow perpendicular to the layers.

One of the classic works on thermal conductivity of fine powders at reduced pressures, as described by Jakob [6], was that of Smoluchowski. The essence of Smoluchowski's

work was that at reduced pressures, gas molecules would experience slip flow in the vicinity of a solid surface. This causes a discernible temperature discontinuity to exist between the solid surface and the gas. When this theory is applied to fine powders, one correctly concludes that many temperature discontinuities are created. These added resistances in turn reduce the transfer of heat through porous powder.

Most of the early works of heat flow through porous material were developed considering ambient or lower temperatures. Few studies were found concerning the flow of heat from one particle to another. One study, by Strong et al. [7], analyzed heat flow through glass fibers at a pressure of 10 $\mu\text{m Hg}$. Even though this investigation worked with materials with smooth surface geometry, its experimental particle-to-particle conductivity was off by an order of magnitude when compared with theoretical values of heat flow perpendicular to the fiberglass rods.

In the first part of the twentieth century, two facts important in insulation were discovered and then investigated. First, it was noted by Smoluchowski [8] that soot had a lower conductance than air. At that time it was thought that the conductivity of air established a minimum value for thermal insulation. However, Kistler and Caldwell [9] in 1934 found that silica aerogel had a thermal conductivity less than air and reasoned that the lower conduc-

tivity resulted from the fact that the pore size of the material was less than the mean free path of molecules of air.

The second important fact, noted by Kistler and described by Wilkes [10], was that when commercial cork was placed in an evacuated chamber, thermal conduction and radiant transfer, through the material, at low temperature, was found to be a small part of the overall heat transfer. This indicated that air was responsible for the majority of the energy transport through the material.

In a more recent study, Peterson [1] showed that successive thin foil radiation shields of low emissivity wound with fine steel wool spacers were exceptionally good insulators, especially when used under vacuum conditions.

Based upon the three developments mentioned above, it was possible to construct super-insulated vessels, at least for cryogenic purposes. The requirements for space age technology placed a premium on lightweight, high efficiency insulation, and, consequently, great interest was shown in cellular and laminated or multi-layer insulation [12, 13]. Most of the development work on multi-layer insulation was done for cryogenic vessels, but some work was performed for high temperature applications. For example, the early design of a thermoelectric nuclear power system for spacecrafts used multi-layer insulation operating at a hot surface temperature of 1285°F [14]. The multi-layer consisted of alternating layers of copper foil with

quartz paper separators, and had an upper temperature limit of 1400°F. The vacuum space was designed and built to hold a pressure of less than 10 μ m Hg for at least five years.

As evident from much of the literature, multi-layer insulation for spacecraft and for cryogenic work was expensive. Prior to the need for super-insulators for spacecraft use, evacuated powders were sufficient for most low temperature purposes. As pointed out by Black et al. [15], although powder insulation does not have as low a thermal conductivity as multi-layer insulation, its advantages are

- 1) it can operate effectively at a few millimeters of mercury or less, thus eliminating the need for high vacuum,
- 2) it can be used in vessels of intricate design, and this eliminates the wrapping and bonding of each component in a vessel, as is necessary with multi-layer insulation,
- 3) it costs less than multi-layer insulation.

In view of this, it seemed that porous powder under partial vacuum should be suitable for terrestrial high temperature insulation applications where weight is not a serious disadvantage.

There is a growing need for efficient high temperature insulation. The present technique used to insulate large, high temperature (200-1000°F) storage vessels is to use thick layers of granular insulation at atmospheric pressure

[16,17]. This approach seems reasonable for large thermal energy storage systems in view of the quantity of energy stored relative to the amount of energy lost. In smaller systems, such as a residential sized thermal energy storage vessel capable of storing 10^6 Btu with minimal losses, the storage efficiency is more closely tied to the overall system size and shape. This results from a smaller volume-to-surface ratio. No references were found concerning high efficiency insulation suited to small systems. Available literature indicates that little consideration has been given to high temperature thermal energy storage systems. It seems that more attention has been directed into developing heat storage media than in developing the heat storage media containment system.

Table 1 has been compiled to illustrate the types of materials, and their associated thermal conductivities, that are available as high temperature insulators. Note that most high temperature insulating materials listed in Table 1 have similar thermal conductivities. This result is not unexpected since these materials are composed of similar materials which is basically SiO_2 . All of the above materials are at atmospheric pressure, with the exception of the diatomaceous earth which is at 1 mm Hg. The reduced pressure results in a thermal conductivity value that is approximately one order of magnitude lower than similar material at atmospheric pressure. Lower thermal conductivities can be obtained as will be explained in the next chapter.

TABLE 1
High Temperature Insulators

Material	Bulk Density (lb _m /ft ³)	Max Temperature (°F)	Thermal Conductivity Btu/hrft° F	
			Mean Temperature @ 500° F	@ 1000° F
Diatomaceous earth, asbestos and bonding material [18]	18	1600	0.053	0.065
Glass blocks, average values [18]	14-24	1600	0.053	0.074
Micro-quartz fiber, blanket [18]	3	3000	0.042	0.075
Rock woll [18]	8-12	—	0.049	0.078
Si1-0-Cell [19] Insulating brick	40	2500	0.142	0.163
Diatomaceous earth, @ 1 mm Hg pressure in air. Nominal particle size 50 μm.	20	1600	0.004	0.010 (est.)

CHAPTER III

THEORETICAL CONSIDERATIONS OF POWDER INSULATION

Introduction

It is relatively easy to measure the overall apparent conductivity* of a powder insulation. However, if one wishes to alter and optimize apparent conductivity other than by increasing thickness, it is necessary to have an acceptable theory with which to proceed. If one idealizes the properties of the media which form the powder and spaces, then one can model its apparent conductivity. Unfortunately, the true geometry is not well modeled by a simple approximation, nor are the properties adequately approximated as ideal. As a result, it is very difficult, perhaps impossible to evolve an analytically tractable model that also accurately describes the phenomena as they occur in the powder. This seems to be the case with modeling of energy transport through porous powder insulating material.

In this study diatomaceous earth (98% SiO_2) was used as the insulating powder. In view of the above discussion the major questions encountered in modeling the irregularly

* Apparent conductivity is heat flow from conduction, convection, and radiation combined and used in equations as if it were conduction alone.

shaped particles were how to describe factors that enhance or impede heat flow through this material. These factors are

- 1) gaseous thermal conduction, as limited by the molecular mean free path and influenced by gas pocket geometry and boundary conditions,
- 2) conduction through solids, limited especially by particle geometry and boundary conditions,
- 3) radiation resistance determined by particle-void space geometry, particle surface properties and boundary conditions.

The best understood of the processes applicable to heat transfer through powders seems to be gaseous conduction, followed by radiation and particle-to-particle conduction. The relative importance of each process is discussed later. The remainder of this chapter is devoted to developing a model for heat flow through porous powder insulation which addresses the above questions.

Theoretical Model

A mechanistic model for heat flow through a porous powder is shown in Figure 2. The total energy flow through the gas-powder mixture is a combination of conductive, convective, and radiant interaction between the solid and gaseous materials present. Symbolically, the total heat flow through the gas powder mixture can be written in functional form as

$$q_T = q_T(q_c, q_r, q_h) \quad (1)$$

For powders with particle size less than 0.2 inches, investigators such as Hill and Wilhelm [20] found no evidence of convection in quiescent, gas-solid beds for conditions of interest to this study. Also, in this work, the powder material was studied at pressures ranging from atmospheric to less than 1 mm Hg. Consequently, convection heat transfer was eliminated from further consideration.

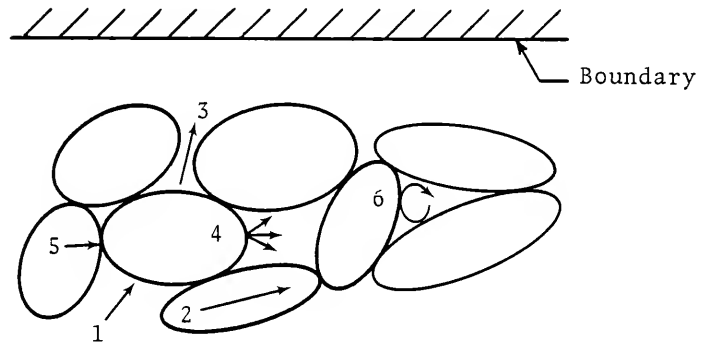


Figure 2

Mechanistic Description of Heat Transfer Through Porous Powder

(1) Gaseous conduction, (2) solid conduction, (3) radiant heat transfer through voids, (4) radiant heat transfer, solid-to-solid, (5) conduction, point contact, (6) convection.

The justification for eliminating convection heat transfer under the conditions discussed above can be shown by estimating the convective heat transfer coefficient, h , between particles. This analysis is given in Appendix B. The results of this analysis reveal that the Nusselt number,

$$Nu = \frac{hb}{k} \quad (2)$$

is of order unity at atmospheric pressure and at temperatures between 250 - 1000°F, then the convective heat transfer coefficient reduces by two orders of magnitude. Hence, convection heat transfer at high temperature and low pressure can be eliminated from further consideration. In view of Equation 2, energy transport through a gas-solid mixture in which convection has been eliminated reduces to primarily a function of conduction. It will be shown later that net radiant transfer contributes only a small fraction of energy transfer under conditions encountered in this work. Thus, Equation 1 is rewritten as

$$q_T = q_T(q_C) \quad (3)$$

The remainder of this chapter is devoted to examining in detail conduction through both gas and solids and the small contribution of radiant transfer through porous powders (silica) under partial vacuum.

Thermal Conductivity of a Perfect Gas

Introduction. This section examines the thermal conductivity of a perfect gas. It is implicit in the use of the property thermal conductivity that a continuum exists. A continuum is assumed to exist as long as the mean free path of a molecule is comparable to the smallest significant dimension of its surroundings. The ratio of the mean free path, λ , of a gas molecule to the average dimension of its boundaries, \bar{d} , is referred to as the Knudsen number. That is,

$$Kn = \lambda/\bar{d}. \quad (4)$$

This number is useful in identifying the conditions under which continuum assumptions apply. The need for identifying whether a continuum exists is important in determining the proper relationship required for calculating the thermal conductivity of a gas. As will be shown in the following sections, the thermal conductivity of a gas in a gas-powder mixture is influenced by the magnitude of the Knudsen number.

Conductivity in a perfect gas. This section examines thermal conductivity of a continuum. A continuum is said to exist when the mean free path of a gas molecule is small ($Kn \ll 1$) compared to the dimensions of its boundaries. For energy transport in a continuum, the gaseous thermal conductivity is given by

$$q_{gc} = - K_g \nabla T \quad (5)$$

The conductivity coefficient, K_g , is given by [21]

$$K_g = \frac{1}{3}(9\gamma - 5) \left(\frac{1}{2} \rho \bar{C} C_v \lambda \right) \quad (6)$$

Density, ρ , is given by

$$\rho = \frac{PM}{R_u T} \quad (7)$$

where P is the pressure, M is the molecular weight of the gas, R_u is the universal gas constant, and T is the temperature of the gas (absolute temperature). The average gaseous molecular velocity, \bar{C} , is given by

$$\bar{C} = \left(\frac{8 R_u T}{\pi M} \right)^{1/2} \quad (8)$$

The mean free path, λ , for a perfect gas is given by

$$\lambda = \frac{R_u T}{\sqrt{2} \pi \sigma^2 A_n P} \quad (9)$$

where σ is the collision diameter of the gaseous molecule, P is pressure and A_n is Avogadro's number.

Specific heat at constant volume, C_v , is given by

$$C_v = R_u / (\gamma - 1) \quad (10)$$

where γ is the specific heat ratio.

Combining Equations 7, 8, 9, and 10 into Equation 6 yields

$$K_g = \frac{(9\gamma-5)}{4(\gamma-1)} \left(\frac{R_u T}{\pi M} \right)^{\frac{1}{2}} \frac{R_u}{\pi \sigma^2 A_n} \quad (11)$$

Equation 11 indicates that gaseous conductivity is a function of temperature and that it should rise with an increase in temperature according to $T^{\frac{1}{2}}$. With an increase in temperature over the range of 250 - 1000°F, and taking into account the temperature variation of C_v and γ , experimental values of thermal conductivity of air at atmospheric pressure change from 0.0192 to 0.0337 Btu/hrft°F.

From Equation 11 one can identify the gaseous molecular properties that will cause the conductivity coefficient to be small. For example, one would choose a gas with high molecular weight, large collision diameter, and a high specific heat ratio. Table 2 lists some values of M , σ and γ for several of the more common gases.

It is interesting to note in Equation 11 that the thermal conductivity of a perfect gas is independent of pressure. Mathematically, the reason for this result is that the direct proportionality of pressure in the density term, ρ , cancels with the inverse proportionality of pressure in the mean free path, λ , expression. Physically, this means that if the density, or number of gas molecules in a given space is decreased, the mean free path or distance between collisions of gas molecules increases so that the transport of energy is unchanged.

TABLE 2

Molecular Weight, Collision Diameter, and Specific
Heat Ratio of Selected Gases

Molecule	M (lb _m /lb _m -mole)	σ [22] (ft x 10 ⁻⁹)	γ [23] [*] (dimensionless)
A	39.948	0.125	1.667
Air	28.97	1.1975	1.40
CO	28.011	1.05	1.40
CO ₂	44.011	1.10	1.285
H ₂	2.015	.886	1.40
He	4.003	.689	1.667
N ₂	28.013	1.23	1.40
O ₂	31.999	1.94 ⁺	1.40
Ne	20.183	1.61	1.667

^{*} Specific heat ratios for gases at low pressure at 80°F.

⁺ Corrected value [24].

The calculation of the thermal conductivity of a gas, as calculated with the perfect gas continuum assumptions, yields results that are adequate for describing real gases in many situations. However, once the variables of temperature, pressure, and boundary conditions are such that a continuum no longer exists, that is $Kn > 1$, then Equation 6 must be modified. This is the topic of the following section.

Thermal Conductivity of a Non-Continuum Gas

As mentioned in the previous section, the conductivity of gases is theoretically independent of pressure in a continuum. However, both Knudsen [25] and Smoluchowski [8] developed theories concerning gaseous thermal conduction for non-continuum. Non-continuum and in the limit free-molecular energy transfer occurs when the confining boundaries of a gas molecule become smaller than the mean free path of the gas molecule. For this condition another phenomenon occurs that limits the energy transfer between a gas molecule and a solid boundary. Knudsen found that when a gas molecule strikes a solid surface that the gas molecule does not necessarily come into thermal equilibrium with the surface. That is, a temperature discontinuity was found between the temperature of the surface and the temperature of the gas molecule leaving the surface. Thus, Knudsen introduced a constant surface property, called the thermal accommodation coefficient, a ,

which is a measure of the degree of energy exchange between a gas molecule and a solid surface. The maximum value of the accommodation coefficient is unity. This value is approached by surfaces that are roughened.

The energy transfer between parallel plates a distance x apart and at moderately low pressure is given by [26]

$$q = \frac{K_g (T_H - T_C)}{x + 2\beta\lambda} \quad (12)$$

where β is

$$\beta = \frac{2-a}{a} \frac{2e}{\gamma+1} \quad (13)$$

and

$$e = \frac{1}{4} (9\gamma - 5) \quad (14)$$

At very low pressures, in the range of molecular conduction, it was found that energy transfer becomes independent of the plate spacing, and proportional to the pressure, P . Rewriting Equation 9 for the mean free path of a gas molecule as

$$\lambda = B/P \quad (15)$$

where

$$B = \frac{R_u T}{\sqrt{2} \pi \sigma^2 A_n} \quad (16)$$

and rewriting Equation 12 in view of Equation 15 for conditions where energy transfer is independent of x yields,

$$q = \frac{K_g (T_H - T_C) P}{2\beta B} \quad (17)$$

Hence, molecular heat conduction is proportional to pressure at very low pressures, ($Kn > 1$).

Equation 17 did not appear suitable for the present investigation for the following reasons:

1. an equation was needed that would be suitable for energy transfer for continuum, transitional, and non-continuum conditions, and not just the latter,
2. the use of Equation 17 requires a knowledge of accommodation coefficients and these values are generally not available,
3. Equation 17 was derived on the basis of parallel plates and the material under investigation is powder material with particles and cavities that are irregular in size and shape and oriented at random; that is, the boundary dimensions must be taken into account.

Strong et al. [7] have found that Equation 6, when modified for non-continuum conditions, gave experimental results that were in good agreement with theoretical predictions

over the range of continuum, transitional, and non-continuum conditions. The material investigated by Strong et al. [7] was fiberglass rods which formed small cavities, as does the powder material of this investigation. The basic assumptions in using Equation 6 were

1. the accommodation coefficient could be approximated as unity, and
2. that by modifying the definition of the mean free path, the equation would be suitable over the range of pressure from continuum to non-continuum conditions.

Since the accommodation coefficient is a measure of the degree of energy transfer between a gas molecule and a solid surface, then it seemed reasonable to conclude that for a material with cavities on the order of the mean free path of the gas, that an effective accommodation coefficient near unit will result. That is, a gas molecule will interact with the boundaries of a given cavity a sufficient number of times to reach equilibrium before escaping to another cavity.

In a non-continuum gas there are two space dimensions that must be taken into account — the mean free path, λ , of the gas molecule and the average space or void dimension of its confining boundaries, \bar{d} . When the mean free path is less than the space dimension, \bar{d} , $Kn < 1$, perfect gas

conductivity is independent of pressure, as expressed by Equation 6. When the mean free path of the gas molecule is close to or greater than the space dimension, $Kn > 1$, then the conduction equation must be modified to take this into account. A modified mean free path of a gas molecule, L , is related to the continuum mean free path, λ , and the gas space dimension, \bar{d} , by Strong et al. [7] as

$$L = \left(\frac{1}{\lambda} + \frac{1}{\bar{d}} \right)^{-1} \quad (18)$$

In the continuum region where $\lambda < \bar{d}$, then

$$L \sim \lambda$$

In the non-continuum region where $\lambda > \bar{d}$, then

$$L \sim \bar{d}$$

To relate the modified mean free path, L , to gaseous conductivity, recall that

$$K_g = \frac{1}{4}(9\gamma - 5) \left(\frac{1}{2} \rho \bar{C} C_v \lambda \right) \quad (6)$$

Substituting Equation 12 into Equation 6 yields

$$\bar{K}_g = \frac{1}{4}(9\gamma - 5) \frac{1}{2} \rho \bar{C} C_v \left(\frac{1}{\lambda} + \frac{1}{\bar{d}} \right)^{-1} \quad (19)$$

where \bar{K}_g is the modified gaseous thermal conductivity coefficient. Equation 19 can now be used to calculate the thermal conductivity of a gas for continuum, transitional, and non-continuum conditions.

Finally, to show that gaseous thermal conductivity, K_g , is related to pressure, recall Equations 15 and 16 and with the appropriate substitution, Equation 19 becomes

$$K_g = \frac{(9\gamma-5)}{4(\gamma-1)} \left(\frac{2R_u}{\pi M T} \right)^{1/2} (1/P\bar{d} + 1/B)^{-1} \quad (20)$$

Thus, as the pressure is lowered, at a fixed void geometry and temperature, the gaseous thermal conductivity decreases monotonically. Note that as the product of $P\bar{d}$ becomes smaller than B , the former value dominates, and it can be concluded that K_g varies essentially linearly with pressure. Conversely, as the product of $P\bar{d}$ becomes large relative to B , K_g is seen to be essentially independent of pressure.

Equation 20 also suggests that the gaseous conductivity will remain the same if, at a given temperature, the modified mean free path, L , is held at a constant value, that is,

$$L = (1/P\bar{d} + 1/B)^{-1} = \text{constant} \quad (18)$$

This means that a given value of K_g can be maintained by either decreasing \bar{d} and increasing P , or by increasing \bar{d} and decreasing P . This suggests that by decreasing the particle size, which will lower the average void dimension, \bar{d} , a higher gas pressure will be acceptable. For example, by selecting particles such that the pressure level is raised from 0.10 mm Hg to 5 mm Hg, while maintaining a constant value of K_g , many of the problems associated with

low pressure, such as the need for diffusion pumps, outgassing of surfaces, and long term leakage, can be avoided or minimized. It is the control over the particle size, and consequently the gas space dimension, that makes a gas-powder mixture attractive for high temperature insulation. Both Equations 17 and 20 indicate that molecular energy transport can be reduced by selecting gases with high molecular weights and high specific heat ratios. This same trend is also exhibited for conduction of heat by gases in a continuum. Equations 17 and 20 do not show a dependency on the collision cross-section in the regime of molecular conduction ($P\bar{d} \ll B$) since the mean free path has been superseded by the confining boundaries of the gas molecule. Also, for non-continuum or molecular conduction, K_g is found to vary with temperature by $T^{-1/2}$. Hence, molecular conductivity decreases as the temperature is elevated.

When the thermal conductivity of a gas has been reduced below the particle-to-particle thermal conductivity in a gas powder bed, little will be gained by further reducing conduction through the gas. Under these circumstances, the particle-to-particle thermal conductivity sets the lower limit of the apparent thermal conductivity through a porous powder under vacuum. (It will be shown later that net radiant transfer appears negligible for the conditions encountered in this study).

The following section examines the contribution of particle-to-particle thermal conductivity to the apparent thermal conductivity of a powder under vacuum.

Particle-to-Particle Conductivity of a Porous Powder

Introduction. Conduction through a region of contact between particles is not easily analyzed except for ideal geometries. For an idealized geometry one may express energy transfer between particles of given size, mathematically define the contact area, and express the proper number of contact points. In most real powders, for example, see Figure 8, page 68, the particles are both irregular in shape and size and oriented at random. These factors make it difficult to determine the parameters necessary to express energy transport by conduction through the powder.

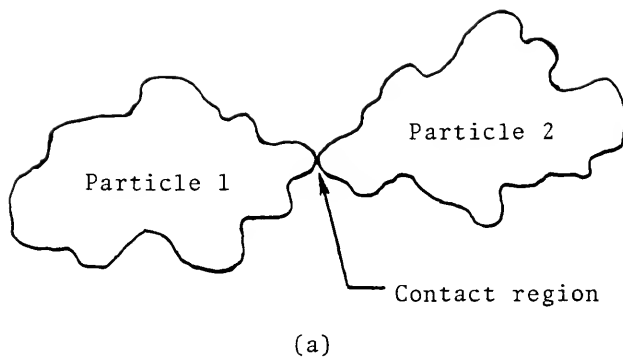
Even with the difficulties of analyzing particle-to-particle conductivity mentioned above, and the fact that there is little in the literature analyzing this topic, it is useful to develop an approximate mathematical expression to describe particle-to-particle conductivity. With a mathematical expression one may readily identify those variables that control the behavior of the material under study.

Theoretical Model. For particle-to-particle conductivity to exist there must be an unbroken path connecting the particles and continuing through them. It is through this path that energy is transferred by solid conduction. A particular problem in analyzing heat transfer through a powder that

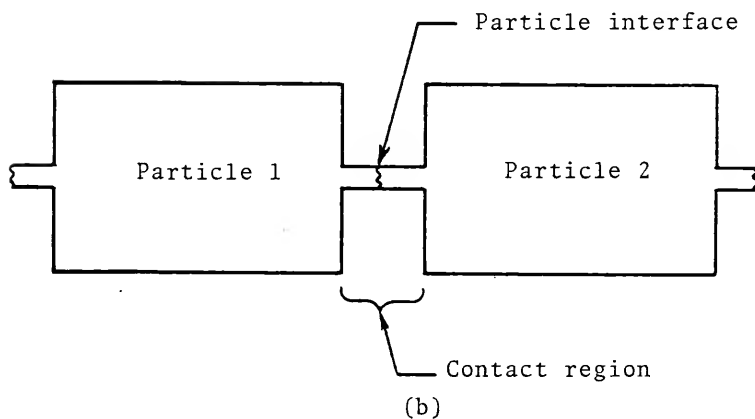
consists of irregularly shaped material, such as the material under consideration in this study, is the difficulty of mathematically defining the path through which energy flows. For example, in Figures 8, 9, and 10 (pages 68 and 69) one sees a variety of shapes ranging from perforated, hollow and solid cylinders to perforated plates, and irregularly shaped solid pieces. With the variety of shapes shown, following the path of heat transfer from particle-to-particle appears to be virtually an impossible task, thus the need for a simplifying model.

In following the path of energy transfer from one particle to the next, one finds that the region of greatest resistance occurs at the smallest area, that is, in a region of contact. If the dimensions of the contact region are small relative to the bulk particle size, then one may approximate particle-to-particle energy transfer in a powder by analyzing the resistance due to the contact region only. This concept is best illustrated by an example.

Consider a cylinder as a particle body as shown in Figure 3. Beside this cylinder is a smaller cylinder which represents the contact region. The two cylinders are in intimate contact and they are aligned on the same axis. Each cylinder has a length to diameter ratio of 10:1 and the size of the two cylinders relative to each other is 100:1. Assuming the conductivity coefficient to be the same



General Particle Shapes In Contact



Idealization Of Particles In Contact

Figure 3

Idealization Of A Contact Region

for both cylinders, one can easily demonstrate that the resistance to heat flow in the smaller cylinder is 100 times that of the larger cylinder. This indicates that the contact resistance, as represented by the smaller cylinder, predominates and that the body resistance of the particles, as represented by the larger cylinder, is negligible. In Chapter V it will also be demonstrated that the relative dimensions of the particle body and contact region are such that a resistance ratio greater than 100:1 is not unusual.

Note carefully that a distinction is made between a contact area and a region of contact. A contact area is the physical area or interface between two particles. A contact region is defined to be the contact area along with the particle materials adjacent to the contact area that restrict energy transfer between two particles forming the contact area. See Figure 3. The contact region is viewed as a continuous path of solid material through which conduction heat transfer occurs even though an interface exist between two particles. This assumption is based upon the existence of sufficient stresses to maintain the two particles in intimate contact. That is,

$$S = F/A \quad (21)$$

where S is the average stress between the particle, F is the force or weight supported by a particle, and A is the contact area between two particles. It will

be demonstrated in Chapter 5 that sufficient stress exists at a contact region to assume intimate, solid contact between particles.

The contact region of a solid particle can be analyzed by any suitable coordinate system. For simplicity, cylindrical coordinates will be used. Assuming constant conductivity, one can express energy conservation in conduction by

$$\frac{\partial^2 T}{\partial r^2} + \frac{\partial T}{r \partial r} + \frac{\partial^2 T}{r^2 \partial \theta^2} + \frac{\partial^2 T}{\partial x^2} + \frac{q'''}{k_s} = \frac{1}{\alpha} \frac{\partial T}{\partial \tau} \quad (22)$$

Since the contact region is small relative to the particle body dimensions, with the latter varying from 1 μm to 100 μm in diameter, the particle material conductivity coefficient, k_s , is assumed to be homogeneous and isotropic. The following assumptions are also made on Equation 22.

1. steady-state,
2. no internal heat generator, and
3. the temperature variations in the r and θ directions are negligible.

A steady-state assumption is made since the material under investigation is intended for use as an insulator operating under steady-state conditions.

The temperature variations in the r and θ directions are considered negligible since the contact region is small relative to the particle body.

With the above assumptions, Equation 22 reduces to a one-dimensional equation and heat flow through a contact region is viewed as quasi-one-dimensional. Thus,

$$\frac{d^2T}{dx^2} = 0 \quad (23)$$

A method of solution for one-dimensional problems in which $q = \text{constant}$ at every cross-section is [27]

$$d[q_x A(x)] = 0 \quad (24)$$

which gives

$$Q_T = q_x A(x) = \text{constant} \quad (25)$$

The x denotes heat transfer in the x -direction and

$$q_x = -k \frac{dT}{dx} \quad (26)$$

Introducing Equation 26 into Equation 25, rearranging and integrating between limits gives

$$Q = \frac{T_H - T_L}{(1/k_s) \int_{x_1}^{x_2} dx/A(x)} = \frac{T_H - T_L}{R_e} \quad (27)$$

where

$$R_e = (1/k_s) \int_{x_1}^{x_2} dx/A(x) \quad (28)$$

and represents the conductive resistance through a contact region. Equation 28 shows that conductive resistance to heat flow is directly proportional to the path length, dx , and inversely proportional to the area, $A(x)$.

An electron microscope photograph of a diatomaceous earth particle, Figures 14 and 15, page 92, shows that the surface of these particles, where contact occurs, has

rounded or smooth geometric features as shown in Figure 4(a). It would appear that the regions of contact could be viewed as hemispherical, cylindrical, conical and so forth. For the purpose of illustration, a hemispherical contact region will be assumed.

A contact region formed by two hemispherical protrusions is shown in Figure 4(a). Note that the area of contact of the hemispherical protrusions has been flattened, as illustrated by the solid line, due to forces imposed on the particles. An equivalent cylindrical heat flow path has been superimposed on the hemispherical contacts. This is to illustrate that the hemispherical contact region is still considered quasi-one-dimensional. The use of a hemispherical contact region serves these two purposes

1. it closely resembles the actual contact region of a particle, and
2. it facilitates the calculations of the contact area with the use of the Hertz formula [28].

The symbols used in analyzing the resistance to heat flow through a contact region are shown in Figure 4(b). Equation 28, written in terms shown in Figure 4(b) is,

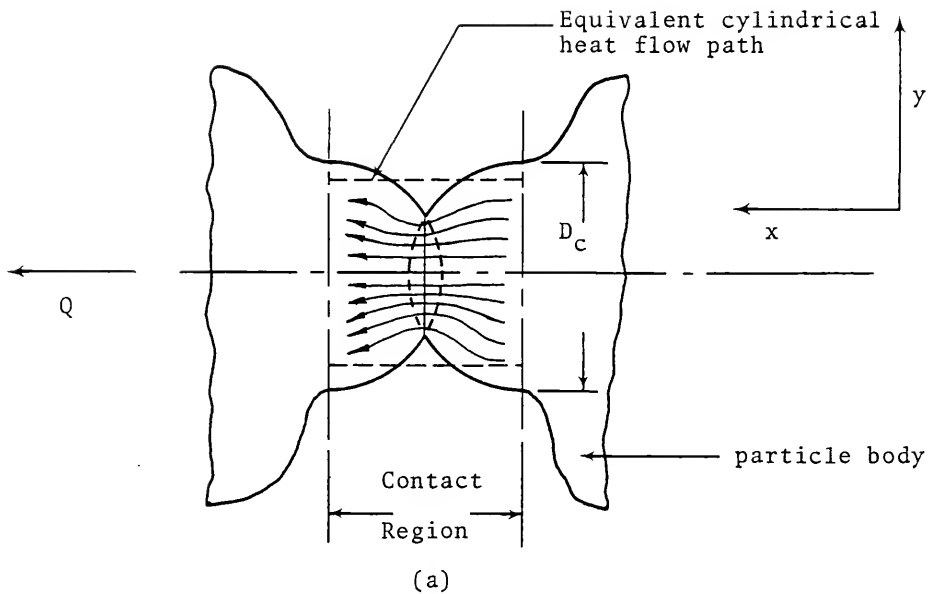
$$R_e = \frac{1}{k_s} \int_{x_1}^{x_2} \frac{1}{\pi y^2(x)} dx \quad (28)$$

The following variable transformations are made.

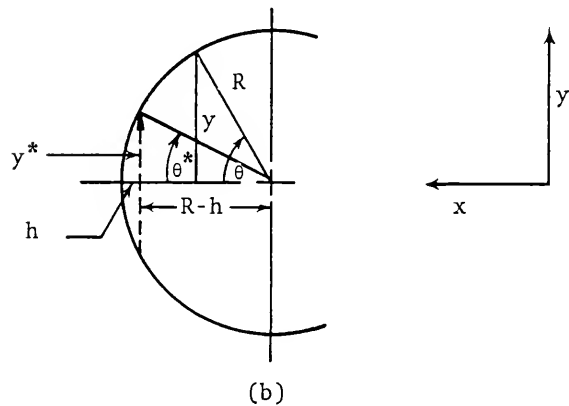
$$y = R \sin \theta$$

$$x = R \cos \theta$$

$$dx = R \sin \theta d\theta$$



Parameters Used in Analyzing Heat Flow Through A Hemispheric Contact Region



Two Hemispherical Projections Forming A Contact Region

Figure 4

Two Particles Forming A Contact Region

Substituting into Equation 28 and simplifying,

$$Re = \frac{1}{k_s \pi R} \int_{\theta_1}^{\theta_2} \frac{1}{\sin \theta} d\theta \quad (29)$$

Evaluating,

$$Re = \frac{1}{k_s \pi R} \ln \tan \frac{\theta}{2} \Big|_{\theta^*}^{\pi/2} \quad (30)$$

and

$$Re = - \frac{1}{k_s \pi R} \ln \tan \frac{\theta^*}{2} \quad (31)$$

The term θ^* represents the angle at which a minimum contact radius, y^* , occurs for a given particle. The contact radius y^* is defined below. Since the contact angle θ^* is less than one degree as calculated using the Hertz formula (see Equation 35), then $\tan \theta^*/2$ can be approximated as

$$\tan \frac{\theta^*}{2} \sim \frac{\theta^*}{2} \sim y^*/2(R-h) \quad (32)$$

Now, Equation 31 is

$$Re = - \frac{1}{k_s \pi R} \ln \frac{y^*}{2(R-h)} \quad (33)$$

Since $R \gg h$, the conductive resistance can be written as

$$Re = \frac{1}{k_s \pi R} \ln \frac{2R}{y^*} \quad (34)$$

The value of y^* represents the radius of the contact area between two hemispheres in contact and it is calculated from the Hertz formula [28] by

$$y^* = \left\{ \frac{3F}{8} \left[\frac{(1-\mu_1^2)/E_1 + (1-\mu_2^2)/E_2}{\frac{1}{D_1} + \frac{1}{D_2}} \right] \right\}^{1/3} \quad (35)$$

where

- F = load per contact
- D_1 = diameter of particle one
- D_2 = diameter of particle two
- μ = Poisson's ratio
- E = Young's modulus

In Equation 35, D_1 and D_2 are diameters of spheres. In this text, the values of D_1 and D_2 represent the diameters of two hemispherical protrusions that form a contact point. Hence, the parameters D_1 and D_2 will be redefined as D_{C1} and D_{C2} , respectively. Generally, these two diameters are not equal but throughout this text the values of D_{C1} and D_{C2} are assumed to be equal and will therefore be written as D_C .

Equation 34 represents the conductive resistance to heat flow through one contact region. Combining Equation 34 with Equation 27 and rearranging results in an equation for heat flow through one contact region. If there are N_h particles in series and N_A particles in parallel, then the rate of heat flow through one foot cube of material can be written

$$Q_T = \frac{n\pi k_s D_C N_A (T_H - T_C)}{2N_h \ln(D_C/y^*)} \quad (36)$$

where

- n = number of contact points per particle
 (heat flow in) for particle in series
 D_c = estimated contact region diameter
 N_A = number of particles per unit of area
 (parallel heat flow)
 N_h = number of particles in a unit of
 height (series heat flow)

The equivalent contact region diameter, D_c , is the estimated diameter of a hemispherical protrusion on a particle. This was shown earlier in Figure 4(a). Also note in Equation 36 that radius, R , has been converted into terms of diameter, D_c .

For a unit temperature difference across a given depth of insulating material, Equation 36 allows one to define an effective coefficient of particle-to-particle thermal conductivity as

$$K_s = \frac{n\pi k_s D_c N_A}{2N_h \ln(D_c/\gamma^*)} \quad (37)$$

The above equations were devised on the basis of an array of uniform particles. However, a material such as diatomaceous earth consists of particles that are non-uniform in size and shape and are oriented at random. Therefore, an empirically determined correction factor, C , must be incorporated into Equation 37. The correction factor will take into account

1. bridging of particle columns,
2. discontinuities in the heat flow path, such as terminated columns,

3. non-uniformity of particle size and shape, and
4. changes in material properties, such as the addition of a foreign substance in a pure base material.

In view of the above, Equation 37 is now

$$\bar{K}_s = \frac{C \pi k_s n D_c N_A}{2N_h \ln(D_c/y^*)} \quad (37)$$

A sample evaluation of the above equation will be discussed in Chapter V.

Equation 37 was derived for application in the contact region connecting two irregularly shaped particles. As a material more closely approximates a sphere, D_c approaches the diameter of the sphere. In this case, $N_A \approx 1/D_c^2$ and $N_h \approx 1/D_c$. Equation 37 can then be written as

$$\bar{K}_s = \frac{C' k_s}{\ln(D_c/y^*)} \quad (38)$$

where

$$C' = C\pi n/2$$

The particle-to-particle conductivity, \bar{K}_s , is seen to depend primarily on the particle conductivity, k_s . The natural log term is essentially a constant for typical variations of the material parameters encountered in this study; that is, for a given powder sample.

The value of C' is a constant for a given material. Incorporated into C' is the value of n , the number of

contact regions leading into a particle.* The value of K_s is seen to vary directly with n . Thus, one should choose an insulating powder so that n is minimized.

Radiant Transfer in a Porous Medium

Introduction. The ratio of radiant-to-total heat transfer in a porous medium has been modeled extensively. However, there is little explicit experimental data, identifying radiation separately, with which to judge the effectiveness of these models. In a porous medium in which the particles are opaque and small ($<10^{-2}$ ft) and in which the temperatures are less than 2700°F , there is agreement in the literature that radiant compared to total heat flow is negligible [29,30].

Radiant heat transfer in a porous powder. In view of the above paragraph, net radiant transfer through powders for conditions encountered in this study was considered to be negligible. The powders used were on the order of 10^{-4} ft in diameter and upper temperature limit was 1000°F . As will be demonstrated in Chapter V, net radiant transfer through diatomaceous earth powder under typical operating conditions accounted for approximately 1%, on a theoretical basis, of total energy transfer. Even though this is

* Contact regions for energy transport out of a particle are considered as a contact region leading into an adjacent particle.

considered to be negligible, a theoretical analysis of radiant heat transfer through powders will be presented for completeness.

The theoretical model presented is similar to those of Argo and Smith [29] and Schotte [30]. To model radiant transport the above authors assumed spherical particles and considered radiant transfer through parallel planes located on each side of a particle. See Figure 5.

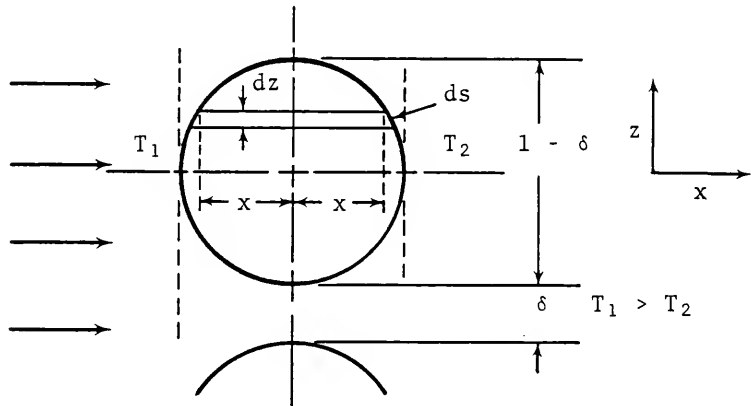


Figure 5

Model for Derivation of Radiant Contribution to Thermal Conductivity through a Porous Medium

The model considers radiant transfer through the voids between particles and radiant transfer from surface to surface in series with the solid particle conduction.

The model also assumes that the particles were opaque and that the particle size was large compared to the wavelength of radiation. Considering the last restriction, the particle size used in this study was 15 - 125 μm . For a temperature range of 250 - 1000°F, Wien's displacement law gives an average wavelength of 7.35 - 3.57 μm , respectively. Thus, the condition is well satisfied with large particles at all conditions, reasonably well satisfied with medium size particles at higher temperatures or small particles at lower temperatures, but is doubtful for the smallest particles at the lowest temperatures.

One may view radiant energy as a packet of energy, or photon, instead of a wave. Of the many photons that participate in radiation passing through a porous powder most will strike the surfaces that form a void many times before they could escape. As a result the probability of absorption is very high compared to the probability of escape. Hence, the effective absorptivity and emissivity may be approximated as unity. By viewing radiant transfer in terms of photons, it is easy to visualize radiant energy transfer as meeting great resistance in flowing through a porous powder, especially for conditions previously described.

The results of the analysis by Schotte [30] give an overall radiative conductivity coefficient of

$$K_r = \frac{1 - \delta}{\frac{1}{k_s} + \frac{1}{k_{rv}}} + \delta k_{rv} \quad (29)$$

where δ is the void fraction, k_s is the solid particle conductivity, and k_{rv} is a particle radiation conductivity coefficient. The latter variable represents radiant heat transfer between a particle and its neighbor. This value will be defined shortly.

The right-hand side of Equation 39 consists of two terms. The first term represents radiant heat transfer to a particle in series with conduction through the particle. The second term accounts for radiation through the void space adjacent to the particle.

The radiative coefficient, k_{rv} , which represents radiative transfer between a particle and its neighbor, is given by Schotte [30] as,⁺

$$k_{rv} = 4\epsilon\bar{d}\xi T^3 \quad (40)$$

where ϵ is the emissivity of the particles, \bar{d} is the average void dimension, ξ is the Stefan-Boltzmann constant, and T is absolute temperature. The temperature used in this equation, T , is the average temperature of the particles. Argo and Smith [29] have pointed out that

⁺ This equation is presented by Schotte [30] as $k_{rv} = 0.692\bar{d}T^3/10^8$. This equation and the one used above are the same.

one investigator [31] used a bulk mean temperature in evaluating Equation 36 and found it in agreement with more elaborate methods for determining radiative transfer through powders.

In summary, the above paragraphs illustrate the role of radiant to total energy transport through a porous powder. The parameters that apparently control radiant heat flow through powders are the particle size, opacity of the material, particle conductivity, void dimension, and boundary temperatures.

CHAPTER IV

EQUIPMENT DESIGN AND MATERIAL PREPARATION

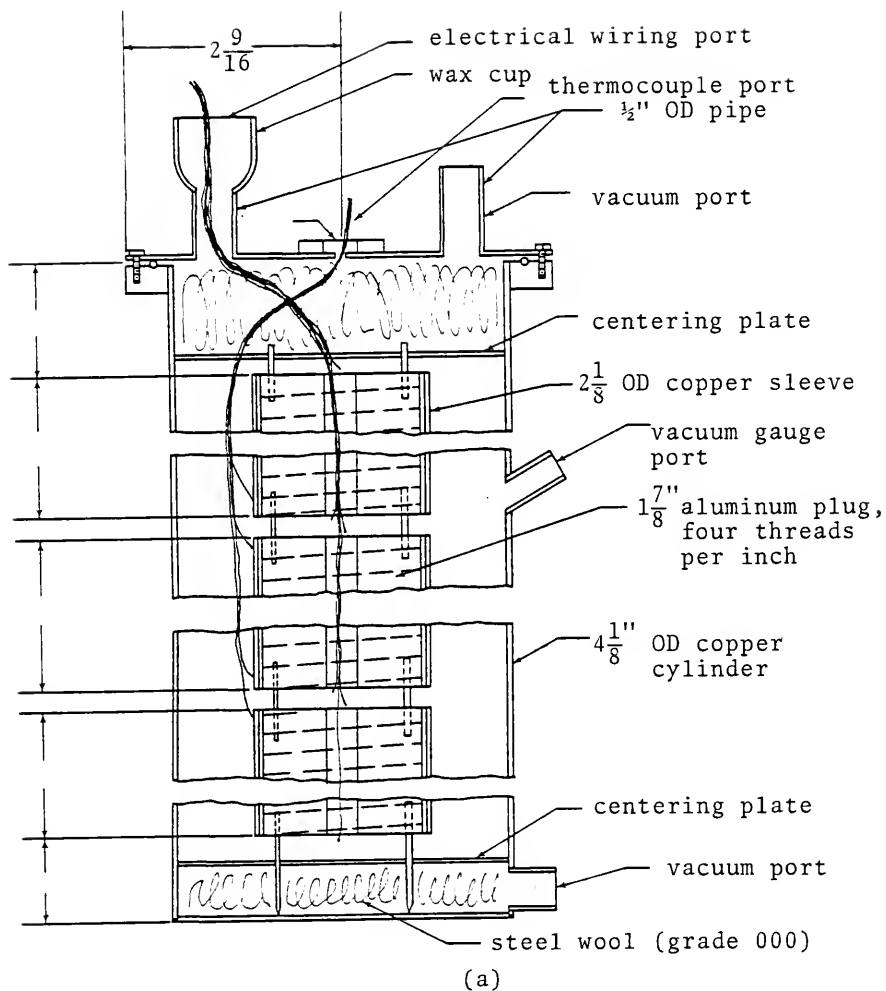
Introduction

The intent of the experimental procedure was two-fold. First, apparent thermal conductivities for various particle sizes were needed to establish the required insulation thicknesses for a high temperature storage system. This required the design and construction of a conductivity test apparatus capable of measuring conductivity of a powder material with a hot face temperature up to 1000°F and for vacuum levels down to 100 μ m Hg.

The second objective of the experimental procedure was to design a prototype high temperature thermal energy storage system using a porous powder under a moderate vacuum ($P \sim 1$ mm Hg) as the insulating material. The thermal energy storage vessel was designed to use an organic oil (corn, cottonseed, peanut, or soybean) as the storage medium.

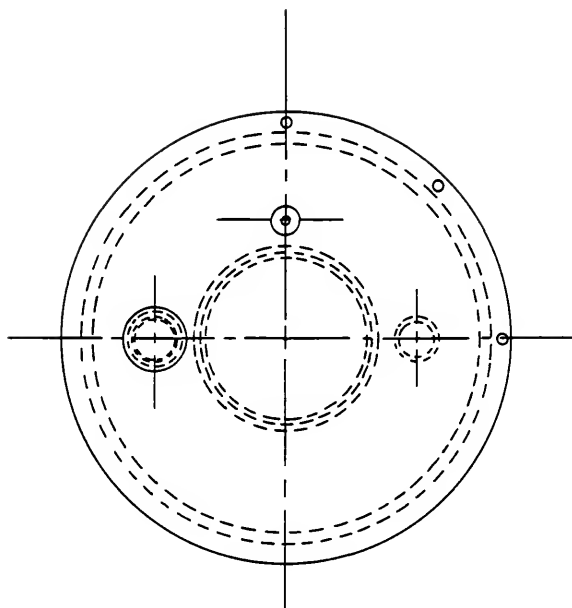
Conductivity Test Apparatus

The conductivity test apparatus is shown in Figures 6(a) and 6(b). The central core of the test cell consists

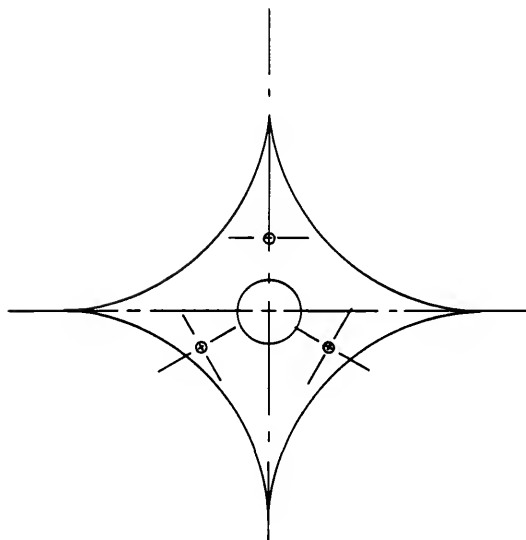


Sectional View Of Conductivity Test Apparatus

Figure 6
Conductivity Test Apparatus

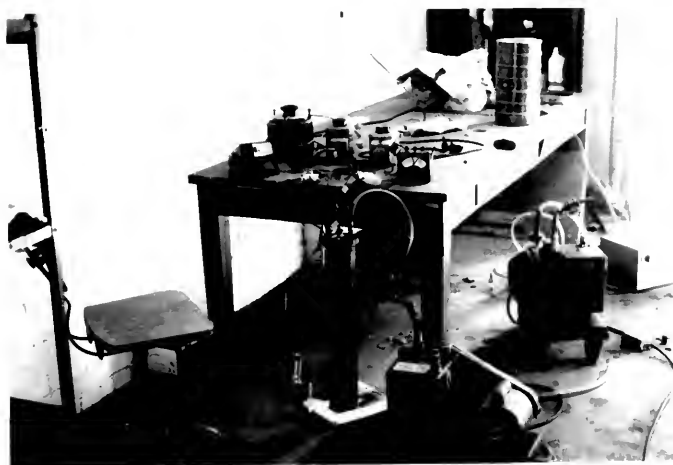


Top View



Centering Plate

Figure 6(a) (Cont'd.)



(b)

Figure 6

Photograph of Conductivity Test Apparatus

of two guard heaters and a center test section heater. The nichrome heater wires were wound on a threaded aluminum core which served to thermally dampen small deviations in the power supply. The aluminum core was wrapped with a ceramic paper and inserted into a copper sleeve. The copper sleeve helped to insure a uniformly heated surface. Chromel-alumel thermocouples were welded to the copper sleeve so that a temperature difference between the guard heaters and the center test section heater could be read. In this manner, the guard heaters could be adjusted to the same temperature ($\pm 1/2^\circ\text{F}$) as the center test section heater, insuring radial heat flow in that section. By measuring the electrical energy dissipated in the central test section, and by measuring the surface temperatures at the boundaries of the powder insulation, the apparent thermal conductivity was calculated. For a cylindrical geometry,

$$Q_{\text{elec}} = \frac{2\pi K_a (T_H - T_C)L}{\ln(r_o/r_i)} \quad (41)$$

Solving for conductivity,

$$K_a = \frac{Q_{\text{elec}} \ln(r_o/r_i)}{2\pi (T_H - T_C)L} \quad (42)$$

For this apparatus,

Q_{elec}	=	rate of electrical energy dissipation
L	=	1 ft test section length
r_o	=	0.163 ft outside radius of insulating material
r_i	=	0.089 ft inside radius of insulating material
T_C	=	average cold surface temperature of insulation at boundary
T_H	=	average hot surface temperature of insulation at boundary

The electrical energy dissipated was calculated by measuring the voltage and current of the center test section heater wires. Thus,

$$Q_{elec} = EI \cos \phi \quad (43)$$

where,

$\cos \phi \approx 1$ (assuming the power factor to be unity for resistance heating)

E = potential

I = current

The value of T_C , the cold wall temperature, was measured on the outside surface of the conductivity test cell. The calculated estimate of the temperature drop across the copper wall was negligible ($< 0.002^\circ\text{F}$). The heat losses through the wires, thermocouples, and electrical conductors had a negligible effect on the test section energy balance, since the temperature difference between

that section and the guard heaters was held to $\pm 1/2^{\circ}\text{F}$ of each other.

Pads of fine steel wool were placed at the top and bottom of the conductivity test cell to facilitate evacuating the fine powder without entrainment. The vacuum ports at the top and bottom of the test cell permitted a faster evacuation time than a single port.

A vacuum port was placed above the upper guard heater and below the lower guard heater so that its presence would not interfere with the center test section. Several different types of vacuum gauges were used during the course of testing.

The first was a thermocouple gauge with a range of one atmosphere to $1\text{ }\mu\text{m Hg}$. However, it was difficult to maintain calibration due to powders infiltrating its sensing element and, consequently, this gauge was not used. A swivel type McLeod gauge with a range of $1\text{ }\mu\text{m} - 5\text{ mm Hg}$ was the second type used. The gauge worked well after a small piece of fine steel wool (0000) was put in line with it to prevent powders from reaching the mercury.

Alignment of the central core of the test apparatus was maintained by a centering plate as shown in Figure 6(a).

Wire feeds were created by packing asbestos string around the wires. The wires were sealed as they passed into the test apparatus by melting high temperature wax around them. The wax had to be re-heated periodically

due to differential expansion between the wire and wax.

The Design of a High Temperature Thermal Energy Storage System

A high temperature thermal energy storage system was designed according to the following criteria.

1. Heat loss per day not to exceed 10 Btu/hrft².
2. The inner tank has a minimum high pressure rating of 150 psi at 700°F.
3. Both the inner and outer tank have low pressure rating at 1.32×10^{-5} psi (100 μ m Hg).
4. The inner tank is capable of holding organic oils.
5. The vessel construction is simple and durable.
6. The vessel requires little maintenance.
7. The inner storage vessel is sized to be compatible with a 6' x 8' concentrating collector.
8. The design potential is intended for mass production at an acceptable cost.

The tank design is shown in Figure 7.

The inner tank was made from a 14 gauge galvanized steel, 42 gallon water tank. Note that one end of the water tank was changed from concave to convex to insure stability at elevated pressures.

The outer tank was constructed from a 14 gauge galvanized steel 200 gallon water tank. The cylindrical

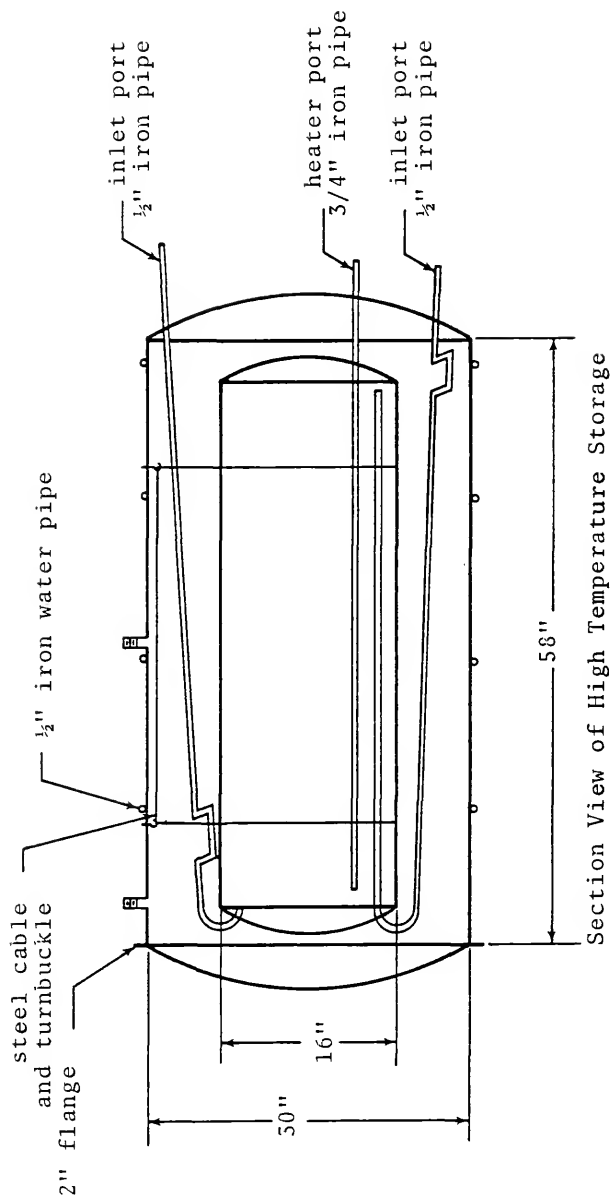


Figure 7

Prototype High Temperature Thermal Energy Storage System

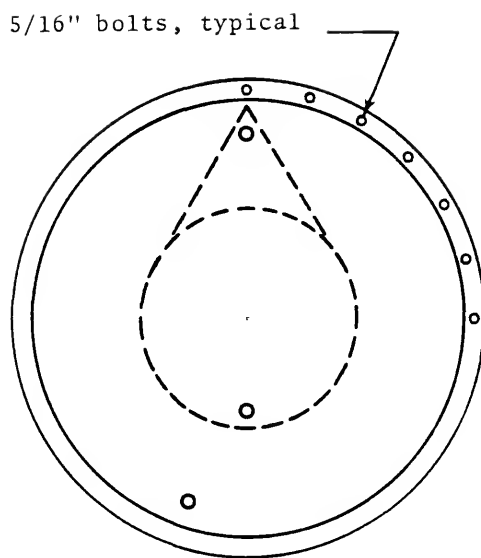


Figure 7(b) (Cont'd)

End View of Tank Showing Internal
Cable Support and Flange Bolt Pattern

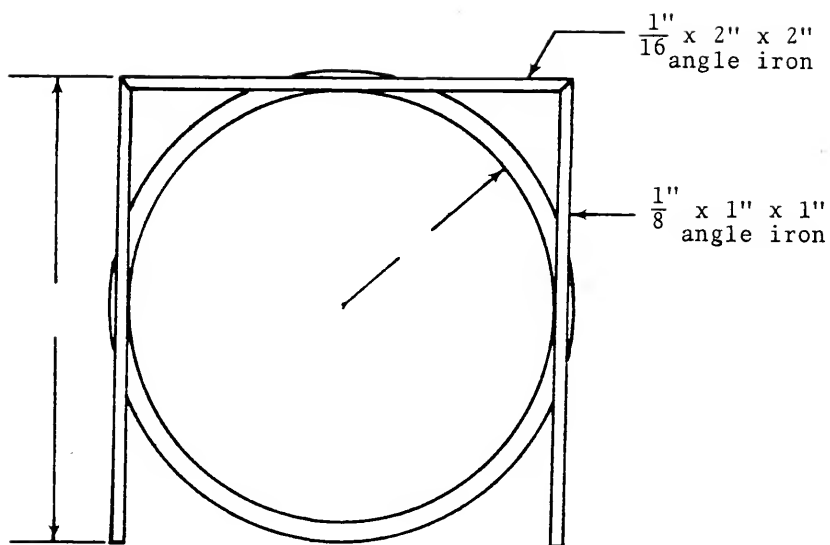


Figure 7(c) (Cont'd)
External Support for Inner Tank



(d)

Figure 7

Photograph of Prototype High Temperature
Thermal Energy Storage System

portion of the tank was shortened and the concave end was changed to convex so that the insulation thickness at the ends of the tanks would be equal to the thickness between the cylindrical portions of the tank.

The inner tank was suspended by two 1/16" diameter stainless steel cables. These cables were selected for their high breaking strength (500 lb. at room temperature) and low thermal conductivity (10 Btu/hrft°F at room temperature). The two cables had sufficient strength at elevated temperatures (1000°F) to afford a safety factor of two (2).

The inlet and outlet pipes were designed with a U-shaped trap which served as an expansion loop and a heat trap. The inlet pipe at the top had the loop placed close to the inner tank so that it would prevent volatile vapors from the organic oil from entering the outlet pipe when the pipe was not in use. The loop on the bottom outlet pipe was placed at the opposite end of its point of attachment and the outlet pipe was sloped downward so that heat conducted through the metal would induce convective flow in the opposite direction, thereby helping to minimize heat flow out of the inner tank.

The rings on the outer tank were needed to meet safety recommendations on externally pressurized tank design [32].

The inner tank was designed to contain organic oils. Copper metal cannot be used with organic oils since these

oils are acidic in nature and react chemically with copper. The long term effect of high temperature organic oils on steel is presently unknown. At low temperatures, steel containers have been used successfully to contain organic oils.

The minimum storage vessel size was estimated for a 6 ft x 8 ft (aperture area) concentrating collector as follows.

$$\begin{array}{l} \text{Heat delivered to} \\ \text{storage system} \end{array} = \begin{array}{l} \text{Heat stored in oil} \\ \text{and its container} \end{array} + \begin{array}{l} \text{Heat losses} \\ \text{from piping} \end{array} \quad (44)$$

Assuming the pipe losses equal 10% of the energy stored in the oil and its container, then

$$H_{in} = 1.10 H_{sto} \quad (45)$$

and

$$I_s A_a \eta_t \tau = 1.1 \rho V C_p \Delta T \quad (46)$$

where I_s is solar insolation, A_a is the collector aperture area, η_t is the collector average thermal efficiency, ρ is density of organic oil (cottonseed), V is the oil tank volume, C_p is the average specific heat of the oil, and ΔT is the temperature rise of the oil.

Solving for volume

$$V = \frac{I_s A_a \eta_t \tau}{1.1 C_p \Delta T} \quad (47)$$

Assuming the following values,

$$\eta_{\tau} = 50\%$$

$$I_s = 300 \text{ Btu/hrft}^2$$

$$\tau = 8 \text{ hr/day}$$

$$\rho = 46.5 \text{ lbm/ft}^3 \text{ @ } 600^\circ\text{F (estimated)}^*$$

$$C_p = 0.66 \text{ Btu/lbm}^\circ\text{F @ } 600^\circ\text{F (estimated)}^*$$

$$\Delta T = 400^\circ\text{F (200 - 600}^\circ\text{F)}$$

$$A_a = 48 \text{ ft}^2$$

and solving for V in Equation 47 yields

$$V = 4.27 \text{ ft}^3 \text{ (maximum)}$$

A 42 gallon tank holds 5.62 ft^3 and afforded an excess capacity to serve as an expansion chamber.

The outer tank size was chosen from commercially available tanks. The most convenient size was a 220 gallon galvanized water tank. The outer tank diameter was 2.5 ft and the inner tank outside diameter was 1.33 ft. Thus, there was a 0.585 ft space for insulation. The ends of the tank were designed to leave an equivalent 0.585 ft space.

A preliminary test on diatomaceous earth powder indicated that an apparent conductivity value of $K_a = 0.01$

* Cottonseed oil data [3]

Btu/hrft°F could be obtained at a hot surface temperature of 600°F, a cold surface temperature of 70°F, and at 1 mm Hg pressure. A 0.585 ft thick layer of insulating powder for these conditions would hold the daily energy loss of the storage tank to approximately 9% per day of the initial energy stored. This approximation is based on changes in temperature and average values of C_v over the interval of temperature change.

Diatomaceous Earth Properties

Diatomaceous earth is the fossilized remains of microscopic marine algae. It consists of approximately 98% SiO_2 (silica). The diatomaceous earth used in this study was purchased commercially. Its intended purpose was for use in swimming pool filters. This material has been used industrially as high temperature, loose fill, insulation and in compressed brick form as a furnace lining. The loose fill material has an upper temperature limit of 1600°F and the brick has an upper limit of 2500°F [19]. The apparent reason for the limitation of the loose fill material is that the powder particles begin to soften at that temperature. This would increase the point-to-point solid conductivity and also cause loss of volume of the material due to settling.

In fine powder insulation it is useful to determine the effect of particle size on apparent thermal conductivity.

One difficulty of determining particle size is that fine powders tend to clump. An explanation for this phenomenon will be discussed later. However, this made it difficult to separate these particles in a sieve and shaker. Grinding these particles in a ball and mill reduced their size but did not make it easier to separate them into various particle sizes.

It was found that the addition of small amount of fine carbon black to the diatomaceous earth, either during the separation process or the grinding process, permitted the powder to separate quickly in a sieve and shaker. The reason for this is that the fine carbon particles act like a lubricant. Carbon particles are shown in Figure 11. Note the puffy appearance of the agglomerated carbon particles. This suggests that the large particles may be comprised of many smaller carbon particles.

A possible explanation of how carbon acts as a lubricant may derive from the fact that carbon is electrically conductive. When the diatomaceous earth particles are vibrated, the particles become charged with static electricity. Hence, if particles have opposing charges, they attract each other. This prevents the particles from passing through the sieve and, consequently, no separation of particles occur. When carbon powder is added to diatomaceous earth, it short circuits the static charge between the particles and this permits the particles to pass through the sieve.

After the diatomaceous earth was separated into its various particle sizes, its geometry remained essentially the same. Figure 8 shows particles trapped in Tyler Sieve #500. Figure 9 shows particles trapped by Tyler Sieve #170. Both of these photographs vividly display the irregular characteristics of these powders.

The various particle size distributions obtained in a sieve and shaker are given in Table 3. The Tyler sieve number corresponds to screen weaves of the following opening size

Tyler Sieve No.	120	170	200	270	325	500	<500
Opening (microns)	125	90	75	53	45	25	< 25

The last category, <500, was simply a catch pan for particles falling through the #500 screen.

The values shown in Table 3 are representative only of the particle sizes in the original diatomaceous earth. These values changed somewhat with each test.

The purpose of generating data for Table 3 was to find the various nominal particle sizes with their corresponding quantities. The variables influencing the separation process were the length of time the shaker was operated and the amount of carbon present. The objective was to use as little carbon as possible. The general results of Table 3 follow.

TABLE 3

Diatomaceous Earth Particle Size and Distribution
Typical Results

Run #	Shaker time (min.)	Diatom. earth (grams)	Carbon (grams)	120	170	200	270	325	500	<500
1	30	174.50	0	62.25	81.75	28.25	-*	2.00	0.25	0
2	10	175.70	1.0	31.55	73.00	45.00	15.25	8.25	2.75	0.90
3	15	190.50	1.0	35.50	11.25	42.00	-*	35.50	49.50	17.75
4	10	188.75	1.5	40.25	12.50	24.50	40.00	32.00	34.50	6.50
5	10	172.00	1.5	25.00	13.75	29.50	47.50	26.50	30.25	1.00
6	10	177.75	2.0	30.75	11.25	23.50	47.25	34.75	29.50	2.75
7	10	179.50	2.0	31.50	10.00	19.50	41.50	38.50	33.75	6.75
8	10	172.75	3.0	29.50	10.75	18.50	37.50	40.75	33.00	5.25
9	8	179.00	4.0	35.50	38.75	63.25	-*	36.50	9.00	0
10	16	178.50	4.0	31.75	10.50	38.00	-*	52.75	49.50	0
11	24	171.75	4.0	32.75	9.25	31.00	-*	27.25	49.75	25.75
12	60	200.25	4.0	32.25	11.00	25.50	-*	29.25	35.25	69.00
13 ⁺	10	326.00	5.0	0	0	21.00	148.00	76.00	81.00	5.00
14 [*]	10	334.50	5.0	18.00	52.00	133.00	111.50	20.00	5.00	0

*This size sieve not used during this test.

+In ball mill for 30 minutes, carbon added at beginning.

•Carbon added after powder pulverized for 1 hour.



Figure 8

Electron Microscope Photograph of Diatomaceous
Earth-Carbon (1% wt) Mixture, Particles from
Tyler Sieve #500 (x 1,000)

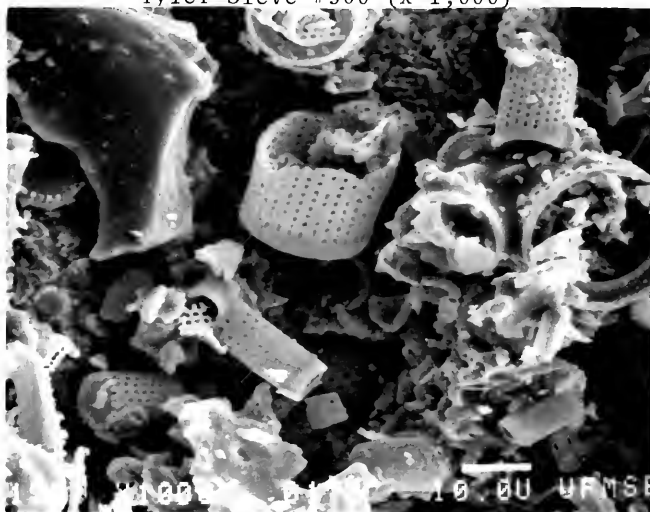


Figure 9

Electron Microscope Photograph of Diatomaceous
Earth-Carbon (1% wt) Mixture, Particles from
Tyler Sieve #170 (x 1,000)

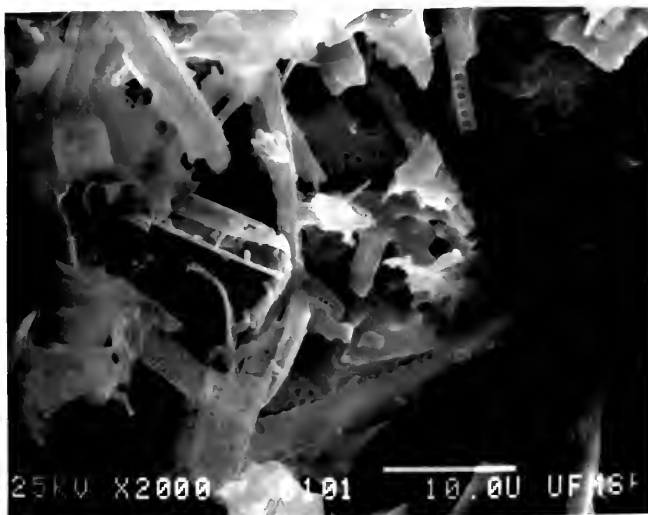


Figure 10

Electron Microscope Photograph of Diatomaceous Earth
(as purchased), x 2,000

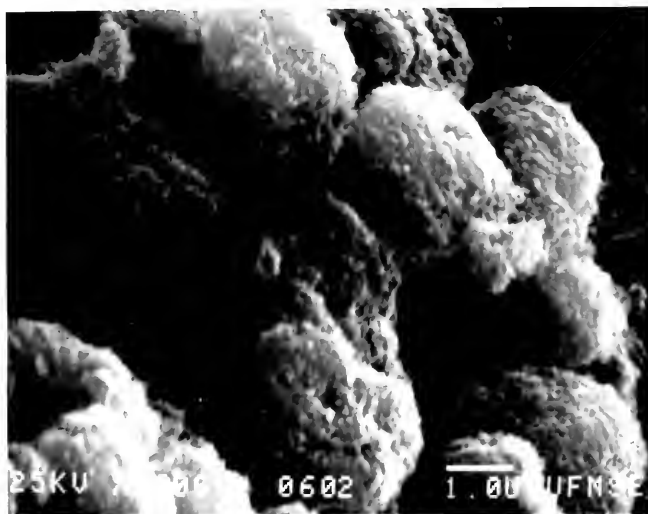


Figure 11

Electron Microscope Photograph of Carbon Black,
Monarch 500 (x 10,000)

1. Run #1 illustrates the difficulty of separating raw* diatomaceous earth. Even after 30 minutes, very few particles were separated.
2. Run #2 illustrates that a large percentage of the particles in the powder are indeed small.
3. The general trend is that as the amount of carbon increased, the greater the percentage of small particles and the faster they separated.
4. A given type of powder with the same amount of carbon and the same shake time shows a general consistency in particle distribution, but some particles of a given size may vary appreciably. Compare Run #4 and Run #5.
5. Carbon added prior to pulverizing diatomaceous earth permits the separation of fine particles in less time than when it was added after pulverizing.

Representative data on density of the various particle sizes are given in Table 4. Note the discrepancy between the measured void fractions[†] and the calculated void fractions. This could be due to air being trapped in and among the particles and not being displaced during the void measurement process. Another explanation, in view of Figures 8 and 9, is that the particles do not separate well and that the mixture of large and small particles causes the void fraction to remain relatively constant.

* Raw diatomaceous earth refers to the material as purchased.

† Void fraction is the ratio of the void space in a container to the total volume of the container.

TABLE 4

Particle Density and Void Fraction of Diatomaceous Earth

Particle Size	Density (lbm/ft ³) [†]	Void Fraction (measured)	Void Fraction (calculated)
Tyler Sieve #120	15.53	-	0.89
" " #170	17.57	0.71	0.88
" " #200	18.98	0.76	0.87
" " #270	19.70	0.71	0.86
" " #325	19.92	0.77	0.86
" " #500	20.08	0.76	0.86
less than #500 (catch pan)	22.67	0.75	0.84
raw diatomaceous earth	17.35	0.83	0.88
carbon black	11.77	-	-
powder for prototype tank	32.84	0.70	0.77
solid diatomaceous* earth (SiO ₂)	145.0		

* Calculated from molecular weight of Si₂O₂.[†] 1% carbon black in powders.

The method used to measure the void fraction and density was to fill carefully a graduated cylinder of known weight with the powder and gently tap the cylinder to settle the particles. The cylinder with the particles was then weighted. The cylinder with the powder was then filled with water to the original level of the powders, and it was then weighed again. With a knowledge of the volume and weight of the powders, a density was then calculated. The void fraction was found by deducing the volume of water required to fill the graduated cylinder to the original volume of powder. The ratio of the latter two quantities is the void fraction.

CHAPTER V

EXPERIMENTAL PROCEDURE AND RESULTS

Conductivity Test Equipment

The conductivity test equipment arrangement is shown in Figures 12 and 13. Power was supplied through rheostats connected to a standard 120 volt AC outlet. Variations in the AC outlet due to daytime peaks were overcome by obtaining a long-term average for the data over a period of several days to more than a week for each datum point. These data were recorded manually.

The test section heaters were monitored for current and voltage. This was accomplished by placing an ammeter on one lead of the heater wire. Voltage was measured on the heater side of the power supply. The guard heater power was monitored only for interest in their power levels relative to the central heater. The guard heater power levels were adjusted to give a temperature within $\pm 0.5^{\circ}\text{F}$ of the central heater. This power level was usually slightly more than the power level of the central heater.

The temperature of the four thermocouples inside the test cell were measured with a digital volt-ohm meter. An ice bath was used as a temperature reference for the

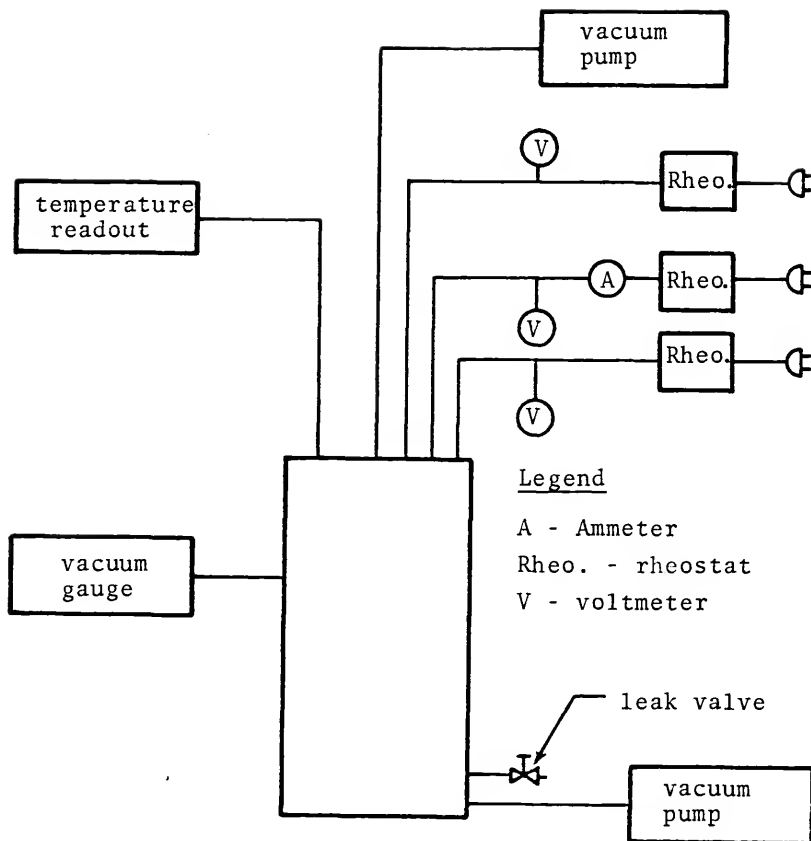


Figure 12
Conductivity Test Equipment Arrangement

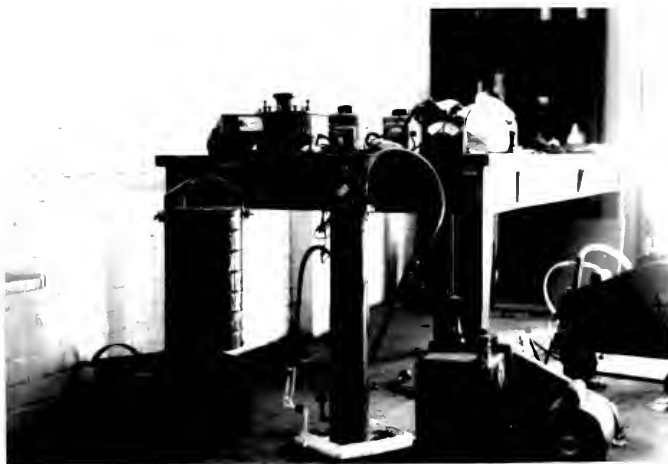


Figure 13
Conductivity Test Equipment

chromel-alumel (Type K) thermocouples. The temperature levels were recorded manually.

A mercury-filled McLeod gauge with a range of 1 μ m - 5 mm Hg was used to measure the vacuum level in the conductivity test cell for data presented in this study. For the preliminary testing period a thermocouple vacuum gauge was used. It was found to lose calibration often and a standard gauge was needed for recalibration. It was found easier to use the standard gauge (McLeod) directly in the experiment.

A common vacuum pump with a blank-off pressure of 15 μ m Hg was used for evacuating the system. A variable leak valve was placed at the bottom of the test cell to regulate pressure.

The objective of this experiment was to find the change in thermal conductivity due to changes in

1. particle size,
2. vacuum level, and
3. temperature levels.

Thermal Conductivity of Powder Insulation Under Vacuum

For the determination of the thermal conductivity of a powder, the thermal conductivity apparatus, as shown in Figure 6, was filled with the powder to be tested. The powders were heated prior to evacuation so that the elevated temperatures would aid moisture removal from the powder particles.

Once the system was thoroughly heated, it was sealed and evacuation was initiated. The heater elements were adjusted so that the main heater and guard heater thermocouples read within $1/2^{\circ}\text{F}$ of each other. This process usually required several days. After a uniform temperature was reached, the system was generally operated under this condition for at least one day to insure that steady-state had been achieved. This additional time was necessary to minimize the effect of the daily changes in the AC power supply and the daily temperature swing of the test room.

During the testing procedure, data were taken manually, usually on hourly intervals, for the three heater temperatures (6 points), outside surface of test apparatus, test heater potential and current, and room temperature.

Data and Results from Thermal Conductivity Test

The experimental values obtained from the thermal conductivity apparatus are shown in Table 5. The four measurements were

1. pressure level, measured in $\mu\text{m Hg}$,
2. the hot surface temperature, T_H , bounding the powder material adjacent to the main heater,
3. the cold surface temperature, T_C , taken on the outside surface of the test apparatus,
4. power dissipated from the central test section heater (potential x current).

From the measured data the apparent thermal conductivity coefficient, K_a , was calculated with the use of Equation 42.

Discussion of Results of Apparent Conductivity Test

Range of values. The range of apparent conductivity values, as seen in Table 5, vary as follows

Highest value: $K_a = 0.0648 \text{ Btu/hrft}^\circ\text{F}$
 @ $T_H = 631^\circ\text{F}$, $P = 760 \text{ mm Hg}$

Lowest value: $K_a = 0.0029 \text{ Btu/hrft}^\circ\text{F}$
 @ $T_H = 340^\circ\text{F}$, $P = 0.6 \text{ mm Hg}$

To put these values in perspective, air has the following experimental conductivity values [33]

Air at 631°F : $K = 0.0272 \text{ Btu/hrft}^\circ\text{F}$
 @ $P = 760 \text{ mm Hg}$

Air at 340°F : $K = 0.0212 \text{ Btu/hr ft}^\circ\text{F}$
 @ $P = 760 \text{ mm Hg}$

From this, the highest test data value, taken at 760 mm Hg pressure, is 2.4 times higher than the conductivity of air, but the lowest value, with a pressure of 0.6 mm Hg, is 7.3 times less than air at 760 mm Hg. This is significant since the conductivity of air is essentially independent of pressure except under the low pressure conditions ($Kn > 1$)

TABLE 5
Average Thermal Conductivity Values
For Evacuated Diatomaceous Earth*

Powder in Tyler Sieve #500 (loose powder)

	Pressure (μ m Hg)	T _H (°F)	T _C (°F)	K _a (Btu/hrft° F)
1	500	405	90	.00364
2	600	733	101	.00648
3	800	700	93	.00750
4	850	330	89	.00483
5	1000	730	104	.00722
6	1000	660	85	.00790
7	1000	558	97	.00444
8	1000	452	87	.00407
9	1000	443	84	.00417
10	760,000	631	192	.06480
11	760,000	432	154	.04600

Powder in Tyler Sieve #500 (powders physically compressed to 45 psi)

12	600	340	97	.00290
13	725	472	85	.00380
14	650	498	100	.00540
15	725	691	100	.00910
16	775	295	86	.00338
17	800	300	84	.00327
18	850	685	103	.00910
19	900	677	102	.00930
20	1000	694	108	.01230
21	1000	746	111	.01130

* Powders contain approximately 1% carbon by weight.

TABLE 5, Continued

Powder in #325 pan (loose powder)

	Pressure (μ m Hg)	T _H (°F)	T _C (°F)	K _a (Btu/hrft F)
22	1400	740	100	.00580
23	1800	462	90	.00475

Powder in #170 pan (loose powder)

24	175	456	81	.00635
25	200	699	88	.00656
26	300	588	108	.00590
27	800	647	110	.00723
28	1000	344	80	.00972
29	1000	531	85	.01198
30	1000	710	98	.01343
31	3800	557	95	.01714

Raw Diatomaceous Earth (No carbon added to loose powder)

32	600	441	93	.00920
33	1000	725	110	.01200
34	2000	545	96	.00980
35	8000	386	110	.02900
36	8000	583	117	.02740

Pulverized Diatomaceous Earth (loose powder)

37	1000	446	99	.00960
38	8000	511	101	.01560
39	8000	715	116	.01448

Air Only

40	760,000	603	235	.07800
----	---------	-----	-----	--------

Fiberglass Cloth and Aluminum Foil - 5 layers

41	400	720	110	.01440
----	-----	-----	-----	--------

discussed earlier. This indicates that a powder under vacuum is effective insulation at elevated temperatures.

The particular area of interest in this study was the conductivity values of the powders near 1 mm Hg, since this vacuum level was within the range of common mechanical vacuum pumps. The conductivities of several of the more thoroughly investigated powders are shown in Figure 16 (page 96). This graph shows the approximate limits and the general trend of the apparent conductivities associated with the large and small grain powders tested.

Radiative transfer. The net contribution due to radiation through a powder insulation, in the temperature range of interest in this study, appears to be negligible. Recall Equations 39 and 40,

$$K_r = \frac{1 - \delta}{1/k_s + 1/k_{rv}} + \delta k_{rv} \quad (39)$$

$$k_{rv} = 4\epsilon \bar{d} \xi T^3 \quad (40)$$

Using typical values in these equations, the resulting coefficient of radiative conductivity is small compared to other modes of energy transfer. For example, using the following values for particles in Tyler sieve #500

$$\delta = 0.76 \text{ (Table 4)}$$

$$\epsilon = 1.0 \text{ (assumed value)}$$

$$\bar{d} = 0.5D = 5.75 \times 10^{-5} \text{ ft.}$$

$$k_s = 0.76 \text{ Btu/hrft}^\circ\text{F (pyrex glass)}$$

and calculating for radiant transfer for powder in a plane adjacent to a hot surface boundary of 1000°F (1460°R) and for a plane at 250°R gives a range of

$$K_r = 0.001 \text{ to } 0.0001 \text{ Btu/hrft}^\circ\text{F}$$

Comparing the above values to a typical apparent conductivities of $K_a = 0.015$ and $0.005 \text{ Btu/hrft}^\circ\text{F}$, shows that radiation accounts for 7% and 2% of the totals, respectively. These values represent a worst case for both temperatures since they were calculated for radiant transfer near the hot surface boundary. For powder near a cold face boundary at $T_C = 90^\circ\text{F}$ (550°R), then K_r represents about 1% compared to an average value of $K_a = 0.01 \text{ Btu/hrft}^\circ\text{F}$. Thus, the net contribution of radiant transfer through a powder for the temperature limits of this study appears to be negligible.

Effective gas conductivity. Note that Equation 20, when rearranged gives

$$\bar{K}_g = \frac{(9\gamma-5)}{4(\gamma-1)} \left(\frac{2R_u}{\pi MT} \right)^{1/2} \left(\frac{1}{P\bar{d}} + \frac{\sqrt{2} \pi \sigma^2 A_N}{R_u T} \right)^{-1}$$

Evaluating with the following parameters for air alone in a container of one foot cubed,

$$\begin{aligned} P &= 760,000 \text{ m Hg} \\ T &= 492^\circ\text{R} \text{ (32}^\circ\text{F)} \\ M &= 28.97 \text{ lb}_m/\text{lb}_m\text{-mole} \\ \sigma &= 1.1975 \times 10^{-9} \text{ ft} \\ \bar{d} &= 1.0 \text{ ft (since } \bar{d} \gg \lambda) \\ \gamma &= 1.39 \\ C_v &= 0.18 \text{ Btu/lb}_m^\circ\text{F} \end{aligned}$$

gives a value of \bar{K}_g of

$$\bar{K}_g = 0.014 \text{ Btu/hrft}^\circ\text{F}$$

and this is in close agreement with published experimental data [34]. However, if Equation 12 is evaluated at higher temperatures, around 600°F, its theoretical values are about 18% below the above cited experimental value.

This discrepancy arises because of the departure of real gases from the assumptions used in deriving Equation 6.

Table 6 has been prepared to show a relative comparison for air and argon when used under non-continuum conditions and at typical mean temperatures encountered in this study. Table 6 suggests that the smaller particle size inhibits gaseous conductivity and that at higher tempera-

TABLE 6

Theoretical Thermal Conductivity of Air and Argon
For Non-Continuum Conditions at $T_b = 860^\circ\text{R}$

Particle Size	Tyler Sieve #170	Tyler Sieve #170	Tyler Sieve #500	Tyler Sieve #500
Gas	Air	Argon	Air	Argon
$d = 0.5 \text{ D (ft)}$	1.625×10^{-4}	1.625×10^{-4}	5.75×10^{-5}	5.75×10^{-5}
$M (\text{lb}_m/\text{lb}_m\text{-mole})$	28.85	39.95	28.85	39.95
$\sigma (\text{ft})$	1.1975×10^{-9}	1.25×10^{-9}	1.1975×10^{-9}	1.25×10^{-9}
$C_V (\text{Btu}/\text{lb}_m^\circ\text{R})$	0.18	0.0748	0.18	0.0748
Pressure ($\mu\text{m Hg}$)	K_a ($\text{Btu}/\text{hrft}^\circ\text{F}$)	K_a ($\text{Btu}/\text{hrft}^\circ\text{F}$)	K_a ($\text{Btu}/\text{hrft}^\circ\text{F}$)	K_a ($\text{Btu}/\text{hrft}^\circ\text{F}$)
10	.00012	.0000753	.000042	.0000268
100	.00111	.000712	.00041	.000262
200	.00211	.00134	.00080	.000513
400	.00381	.00241	.00154	.000983
600	.00522	.00328	.00222	.00143
800	.00640	.00399	.00286	.00181
1,000	.00740	.00460	.00345	.00218
2,000	.01078	.00661	.00588	.00368
4,000	.01398	.00846	.00907	.00561
8,000	.01642	.00983	.01246	.00759
10,000	.01701	.01016	.01346	.00816
50,000	.01923	.01138	.01815	.01080
100,000	.01955	.01156	.01897	.01124
380,000	.01979	.01169	.01963	.01167
760,000	.01983	.01171	.01975	.01167

tures, argon performs significantly better than air, especially in the pressure range of interest (0.50 μm to 10 mm Hg). Carbon dioxide has a lower thermal conductivity than air, but its values are not as low as those of argon. In checking these values with Equation 12, keep in mind that the theoretical conductivities at ambient pressures tend to fall as much as 20% below experimental values, as the temperature is raised from 32 to 600°F. It is not apparent if this deviation continues at reduced pressures.

This nominal diameters used in evaluating the powder particles were taken as the average of the screen openings below and above the trapped powder. For example, if powders were trapped between Tyler Sieve #500, screen opening 25 μm , but passed through Tyler Sieve #325, screen opening 45 μm , then the nominal particle size was taken as the average of the two values, or 35 μm . It is well to point out that the nominal diameter is used for convenience in discussing the particles.

Average void diameters of 50% of the nominal diameter were assumed in view of Figures 8 and 9 and from observation of diatomaceous earth particles under an optical microscope. At the onset of this study it was assumed that powders separated by sieves would be of fairly uniform size. However, Figures 8 and 9 indicate that the nominal size, as defined above, is larger than many particles found in the powders.

Particle-to-particle conductivity. Table 4 (page 80) shows a variety of vacuum levels, hot face temperatures, and apparent thermal conductivity values for powder insulation under vacuum. These values were obtained from typical operating conditions of a high temperature thermal energy storage system. With the experimental data of Table 5, and by recalling that energy transport through powders under vacuum occurs principally by conduction, one may use the developed theoretical equations to proportion heat flow through gas and particle-to-particle conduction. This will be done in the following paragraphs by evaluating the conductivity coefficients, K_g and K_s .

Table 7 illustrates the proportioning of apparent conductivity into gaseous and particle-to-particle conductivity. The gaseous conductivity, K_g , was calculated from Equation 12 and the apparent conductivity values, K_a , were taken from Table 5. The particle-to-particle conductivity was then calculated from these values using the estimated area ratios. As a result of viewing the diatomaceous earth powders under an optical microscope, a parallel heat flow model, in the low pressure range, was selected. The gas and solid materials were viewed as parallel tubes. Heat flows through the separate tubes composed of different materials, in parallel. This can be expressed as

TABLE 7
Proportioning of Thermal Conductivity
Into Gaseous and Solid-to-Solid Conductivity

<u>Small Grain Particles</u>					
Line*	T _b (°F)	P (μm Hg)	K _a * (Btu/hrft°F)	K _g (Btu/hrft°F)	K _s (Btu/hrft°F)
1	247.5	500	0.00364	0.00204	0.0316
2	417.0	600	0.00648	0.00239	0.0319
3	396.5	800	0.00750	0.00286	0.0364
4	209.5	850	0.00483	0.00327	0.0145
5	417.0	1000	0.00722	0.00343	0.0308
6	372.0	1000	0.00790	0.00348	0.0357
7	327.5	1000	0.00444	0.00355	0.0103
8	269.5	1000	0.00407	0.00363	0.0068
9	263.5	1000	0.00417	0.00364	0.0075
10	411.5	760,000†	0.0648	0.01988	0.3445
11	293.0	760,000	0.0460	0.01850	0.2172
<u>Large Grain Particles</u>					
24	268.5	175	0.00635	0.00202	0.0378
25	393.5	200	0.00656	0.00211	0.0388
26	348.0	300	0.00590	0.00307	0.0264
27	378.5	800	0.00723	0.00642	0.0131
28	212.0	1000	0.00972	0.00758	0.0252
29	308.0	1000	0.01198	0.00750	0.0445
30	404.0	3800	0.01343	0.00739	0.0572
31	326.0	600	0.01714	0.01352	0.0434

* From Table 5.

† 760,000 μm Hg equals one standard atmosphere.

$$q_T = q_{gc} + q_s \quad (48)$$

This results in,

$$K_a = \frac{A_{gc}}{A_T} \bar{K}_g + \frac{A_s}{A_T} \bar{K}_s \quad (49)$$

The area fractions of the above equation would be a difficult parameter to measure for a loose powder. These values can be estimated under the assumption that the area ratios can be deduced from the void ratio. For example, if all of the loose powder material in a unit cube were separated into a uniform solid in the bottom of the cube, with the void volume (residual gas space) above it, then the ratio of the void volume to total volume equals the void ratio. Since the cube is of unit width, the void will equal the area ratio as given in the first term on the right-hand side of Equation 49. The same reasoning will also apply to the solid ratio which is the ratio of the solid volume to total volume or the solid area to the total area, as seen from the edge of the unit cube. Hence, for a differential thickness of powder, the projected solid and void areas will, on the average, be equal to the solid ratio and the void ratio, respectively.

In reviewing Table 5, one would generally expect a relationship between particle-to-particle conductivity and

temperature. This relationship certainly exists, but is not readily apparent as it is masked by the pressure sensitive gaseous conductivity. This is evident in Lines 4-5 of Table 5. These values suggest the need for more detailed information -- particle sizes, void dimensions, and so forth. Also, the temperature gradient, particularly near the hot face boundary, influences the overall apparent conductivity. [Typical temperature profiles are shown in Figure 22.] For amorphous powder particles with an increasing value of particle conductivity, k_s , the conductance next to the hot face boundary will be significantly more than throughout the remainder of the material.

One particular difficulty in working with powders is that the value of its solid particle conductivity, k_s , is not available. An obvious choice as a substitute for k_s of diatomaceous earth would be to use the conductivity coefficient for another amorphous material, such as that of pyrex or quartz glass. The reason for selecting these materials is that the electron microscope photographs reveal particles that show cleavage planes characteristic of an amorphous material. Evidence of crystallinity was not apparent. Also, the data reported herein indicate that point-to-point solid conductivity increases with temperature, and this is consistent with amorphous material such as pyrex or quartz glass.

Equation 37 can now be evaluated for particle-to-particle conductivity. Recall Equation 37,

$$\bar{K}_s = \frac{C k_s n \pi D_c N_A}{2N_h \ln(D_c/y^*)} \quad (37)$$

where,

$$y^* = \left\{ \frac{3}{8} F \left[\frac{(1 - \mu_1^2)E_1 + (1 - \mu_2^2)/E_2}{1/D_1 + 1/D_2} \right] \right\}^{1/3} \quad (38)$$

The above equations will be evaluated based on the following assumed values for a one foot cube sample of Tyler Sieve #500 particle (nominal diameter $D_n = 1.5 \times 10^{-5}$ ft) at a mean temperature of 400°F.

$$k_s = 0.76 \text{ Btu/hrft}^\circ\text{F (pyrex glass)}$$

$$n = 1 \text{ contact point per particle (heat flow in)}$$

$$N_h = 1/\frac{1}{2} D_n \sim 1.33 \times 10^5 \text{ particles/ft}$$

$$N_A = (1/\frac{1}{2} D_n^2)^2 \sim 1.78 \times 10^{10} \text{ particles/ft}^2$$

$$F = (2/3)(20.0 \text{ lbf/ft}^2)/1.78 \times 10^{10} \text{ particles/ft}^2 \\ = 7.5 \times 10^{-10} \text{ lb}_f$$

$$\mu_1 = \mu_2 = 0.25$$

$$E_1 = E_2 = 10 \times 10^6 \text{ lb}_f/\text{in}^2$$

$$D_c = D_1 = D_2 = 3.3 \times 10^{-6} \text{ ft (estimated equivalent diameter of contact region.)}$$

Note in the above values that the particle size has been estimated as 1/2 the nominal particle size. The weight of force, F, is taken at 2/3 the depth of the powder

bed, and the force is divided by the number of points of contact that support it. In this case a value of unity has been assumed. This will be explained later. The value of D_c was estimated from Figure 14 and for this example all particle contact points are assumed to have the same value.

With the above values, Equation 37 gives

$$K_s = C(0.09) \text{ Btu/hrft}^2\text{°F}$$

The correction factor required is on the order of unity. This is consistent with values of solid conductivity shown in Table 6 for particle-to-particle conductivity values obtained at low pressure.

The average stress holding two particles in contact for the conditions listed above is found with the use of Equations 21 and 35, to be

$$S = 2.1 \times 10^4 \text{ lb}_f/\text{in}^2$$

This value appears to be more than sufficient to maintain two particles in intimate, solid contact. It is on this basis that the contact area resistance was replaced with a contact region conductive resistance.

The two values at atmospheric pressure suggest that other factors affect heat transfer at that pressure level. One avenue that may be explored is that at conditions where

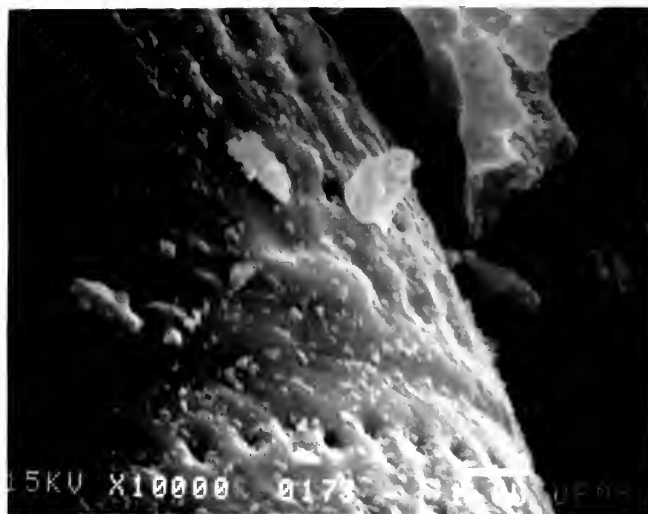


Figure 14

Electron Microscope Photograph of Surface
of Diatomaceous Earth Particle, Tyler Sieve #500
(x 10,000)

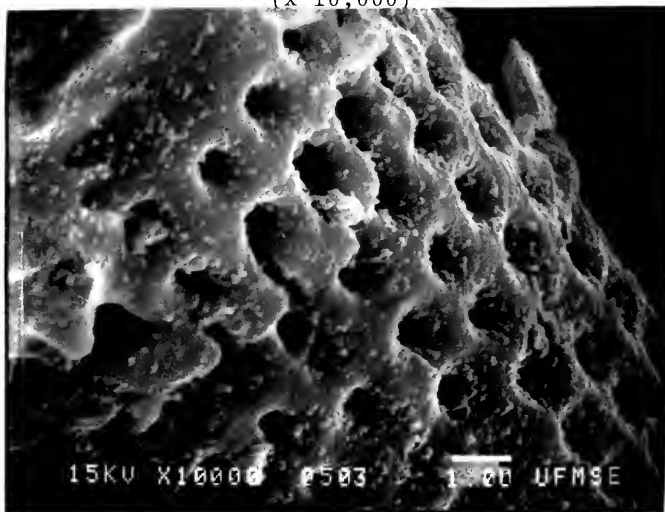


Figure 15

Electron Microscope Photograph of Surface
of Diatomaceous Earth Particle, Tyler Sieve #170
(x 10,000)

continuum assumptions apply, $Kn \ll 1$, a series-parallel model may be more applicable. Since the analysis of energy transport through powders at atmospheric pressure was beyond the scope of this study, this topic was not pursued.

In the sample calculation, the number of contact regions, n , was assumed to be unity. This value was selected after inspecting the particles in an optical microscope which gives a three as opposed to a two-dimensional view as seen in the electron microscope photographs. In three dimensions the diatomaceous earth particles look much like an assembly of tinker toys. The particles adhere in groups and these groups are separated with thin columns of particles. These columns appear like small magnets clinging together. Within the groups, it appears as though the individual particles are repelling each other. This separation of particles reduces the number of contacts between particles. For example, small pebbles form piles in which each higher pebble is supported by several lower pebbles with several points of contact. Because of the formation of groups, separated by strands, diatomaceous earth particles seem to minimize the number of contact regions without breaking apart. In the following paragraphs, the cause of this arrangement is discussed.

The force of attraction between particles is thought to be electrostatic in origin. In that sense, it is similar to polished metals which adhere to each other. The diatomaceous earth particles do not appear to interlock

as do pebbles (uncharged particles). It was thought that water surface tension would be a factor in particle adhesion. However, heating the particles, to drive off moisture, did not appear to alter their attraction, at least at atmospheric pressure.

When the diatomaceous earth particles were viewed under an optical microscope and the glass support was vibrated by tapping, the individual particles did not vibrate. This is in contrast to similar observations of aluminum powder particles, which have no electrostatic forces. The absence of induced vibrations implies a force of attraction between the particles.

One can see from Equation 35 that the effect of a force or weight on porous powders is two fold. First, it increases the contact diameter. This effect is small as evidenced by the log term in the denominator. Second, and more significantly, increased force presses more particles together and as a result a larger number of contact regions form. This net effect of weight on \bar{K}_a , as shown in Figure 16, contrasts the curves for Tyler Sieve #500 powders for compressed and uncompressed material. Note that the effect of compressing the powder at lower temperatures is to decrease its thermal conductivity as compared to uncompressed particles. Presumably, this occurs because of a decrease in the thermal conductivity of the gas that results from a reduced void dimension in the non-continuum regime.

At higher temperatures, on the other hand, the apparent conductivity of the compressed powders increases rather sharply. Nevertheless, Figure 16 suggests that compressed powders may be used to support a storage tank weight without a large penalty in insulation performance. Specifically, fine compressed powders can be placed under a container for support and loose, uncompressed powders can be placed in the remaining volume. In this manner only limited supports or no supports at all are needed to separate the internal and external tank. This eliminates the need for large internal or external supports through which heat may be lost.

The apparent thermal conductivity values of Table 5 have been reviewed except for the last four categories: raw diatomaceous earth, pulverized diatomaceous earth, air only, and fiberglass cloth and aluminum foil. The raw diatomaceous earth appears to perform similar to the powder in the #170 pan. That is, the powder particles and the average void dimensions are large. Pulverizing the raw diatomaceous earth and using it without separating it into different particle sizes will be of some advantage.

The air-only condition was measured to demonstrate the effect of using air alone without convection suppression or radiation shielding.

The fiberglass cloth and aluminum foil demonstrate a value that one might expect from this material. The one

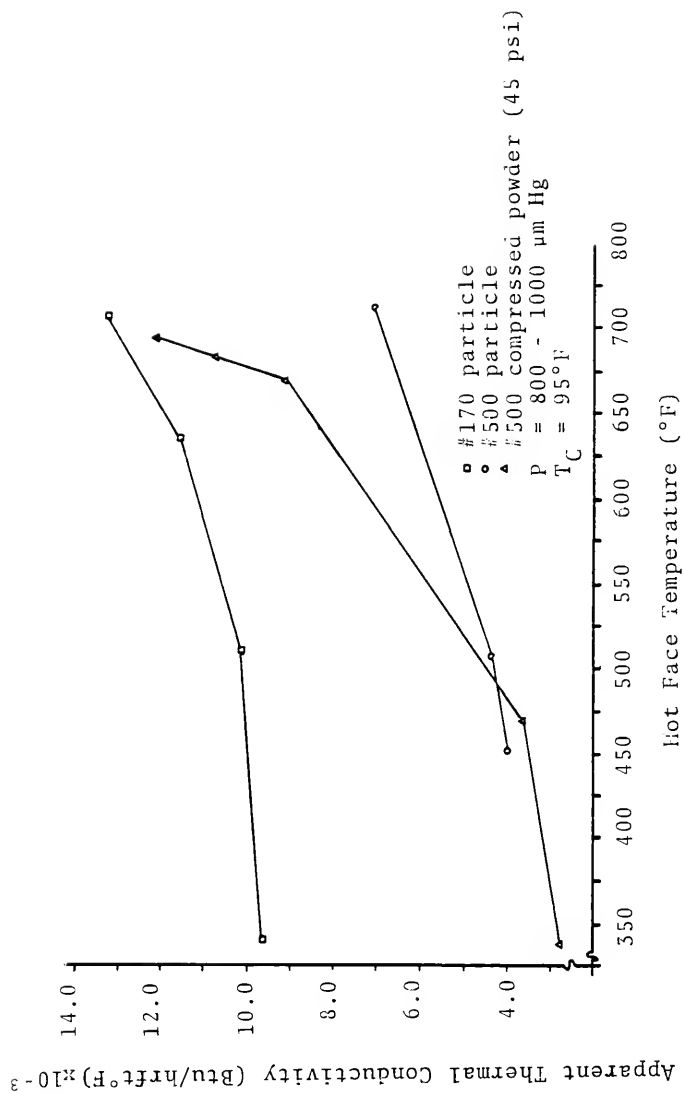


Figure 16

Apparent Thermal Conductivity of Selected
Diatomaceous Earth - Carbon (1% wt.) Particles

value given in Table 4 is relatively high, but it can be made somewhat lower by using more layers of fiberglass cloth and aluminum foil. However, note that this multilayer material is at a pressure of 0.40 mm Hg. To produce a significant drop in K_a for this material, the pressure must be reduced to a level of 0.10 mm Hg or less. See Table 5, page 79.

The fiberglass cloth and aluminum foil were difficult to put together since the multi-foil layers were individually wrapped. Some of the problems with wrapping the insulation were

1. the need for securing the layers so that they did not unravel,
2. a support system was required to separate the inner and outer tank, and
3. the supports and piping to and from the inner tank had to be carefully wrapped to prevent heat loss.

It is well to point out that multi-foil insulation at low pressure works well. But, its complexity and expense make it an unlikely candidate for routine high temperature use.

Effect of particle size in a non-continuum. Figure 16 (page 96) illustrates the trend of particle size versus conductivity. The larger particles, in the case from Tyler Sieve #170, pass heat about three times more readily than the particles of Tyler Sieve #500. This trend is also seen in the cryogenic region [10]. The apparent reason for this

is that small powders suppress gaseous conductivity more effectively and they create a greater resistance to heat flow due to contact region resistance as explained in Chapter 3. It is interesting to note the behavior of the compressed powder (Tyler Sieve #500) in Figure 16. At the low temperature end of the graph the compressed powders have a high resistance to heat flow due to non-continuum conditions created by the fine particles. However, at higher temperature, the conductivity increases rapidly. It is assumed that this is due to the presence of additional solid material through which heat may pass. This powder was compressed to about one half of its original volume. The above observation is consistent with Equation 37 in which heat flow is directly proportional to the number of particles, N_A .

Effect of vacuum level. The vacuum level has a major impact on the heat loss characteristic of the powder insulation under vacuum. Figure 17 is a theoretical curve showing the characteristic decline of gaseous conductivity for air and argon. The decline is seen to be linear at points less than 1000 $\mu\text{m Hg}$. The gaseous conductivity below this pressure varies asymptotically with pressure. Note the relatively flat response at pressures near 10,000 $\mu\text{m Hg}$ (10 mm Hg) in Figure 17. This indicates the importance of operating evacuated insulation at less than 10 mm Hg.

Figure 17 illustrates the trend in the gaseous conductivity for air and argon at pressures below 10 mm Hg

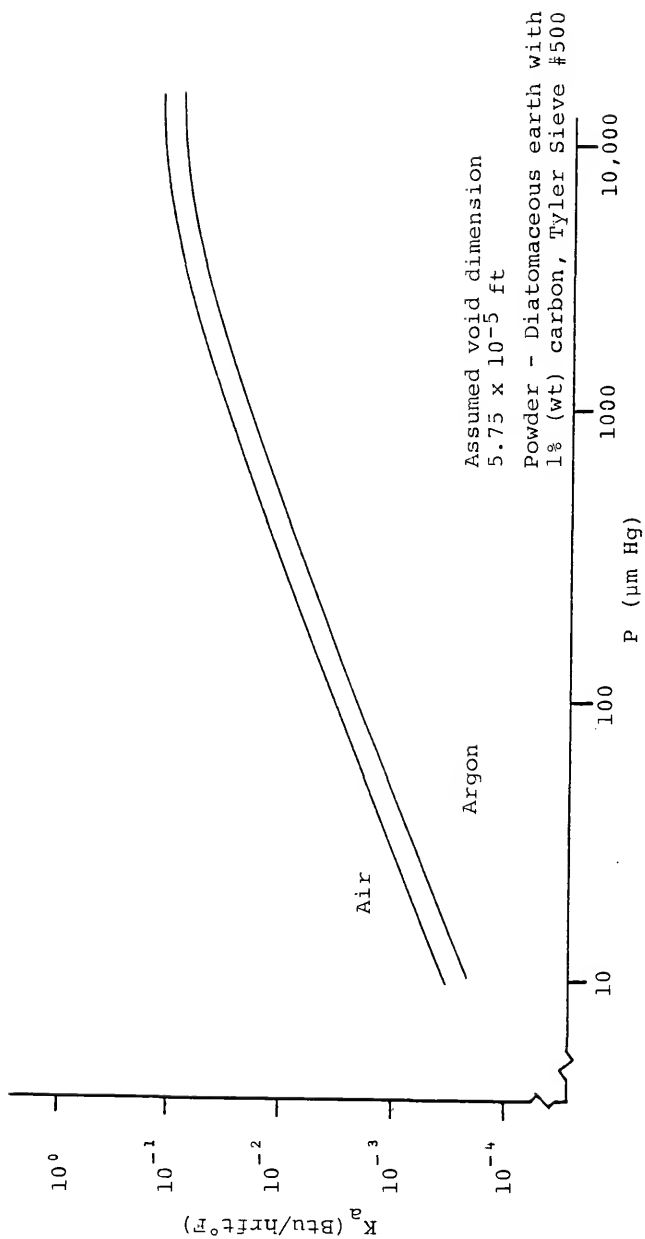


Figure 17

Gas Conduction vs Gas Pressure in Powders
 Under Vacuum (Theoretical)

where a rapid decline in conductivity occurs. On this scale, a recommended operating range falls between 0.5 mm Hg to 3 mm Hg since these values are easily obtained with common mechanical vacuum pumps.

Selection of a particular operating pressure will depend upon the particle size, particle material, residual gas present, temperature level, cost of stored energy and so forth. A pressure much lower than 0.5 mm Hg can be used but at the expense of more complex vacuum pumps (diffusion or molecular pumps), longer pumping times, and potential problems of outgassing. From theoretical considerations a point will be reached in which further reductions in heat loss through gas conduction becomes negligible compared to solid particle conduction losses. This investigation did not experimentally identify this pressure region due to equipment limitations. However, part of the goal of this work was to identify a practical upper limit for pressure commensurate with a low coefficient of thermal conductivity ($K < 0.015 \text{ Btu/hrft}^\circ\text{F}$ (@ 1000°F). The pressure range of 0.5 mm Hg to 3.0 mm Hg is designated as an upper pressure range for accomplishing this goal.

Effect of carbon and iron in diatomaceous earth. Carbon was added to the diatomaceous earth, at about 1% by weight, to enhance pouring and separating characteristics of the latter. Very small amounts of steel powder found its way into the material that was pulverized in a ball mill. [The

ball mill container and rollers were made of steel.] From the limited data of Table 5, it appears that neither the carbon nor fine steel had a significant measurable effect on the thermal conductivity of diatomaceous earth.

Thermal Energy Storage System

The thermal energy storage system was filled with approximately 500 pounds of diatomaceous earth that had been pulverized in a ball mill for 30 minutes. Approximately 1% by weight of carbon black was added prior to pulverizing since the carbon was found to give the diatomaceous earth better pouring characteristics. A small amount of raw diatomaceous earth, 50 pounds, had to be used to completely fill the tank. This material was located in the top back section of the tank and no observable temperature difference in this area was noticed during the test.

The tank was filled by first evacuating the insulation space and then letting the powders be pushed into the tank as atmospheric pressure filled the annular void. This procedure was much quicker and easier than trying to fill the insulation space by hand. It was also found that better packing and distribution of the insulation material was obtained since no hot spots were noticeable on the exterior of the outer tank.

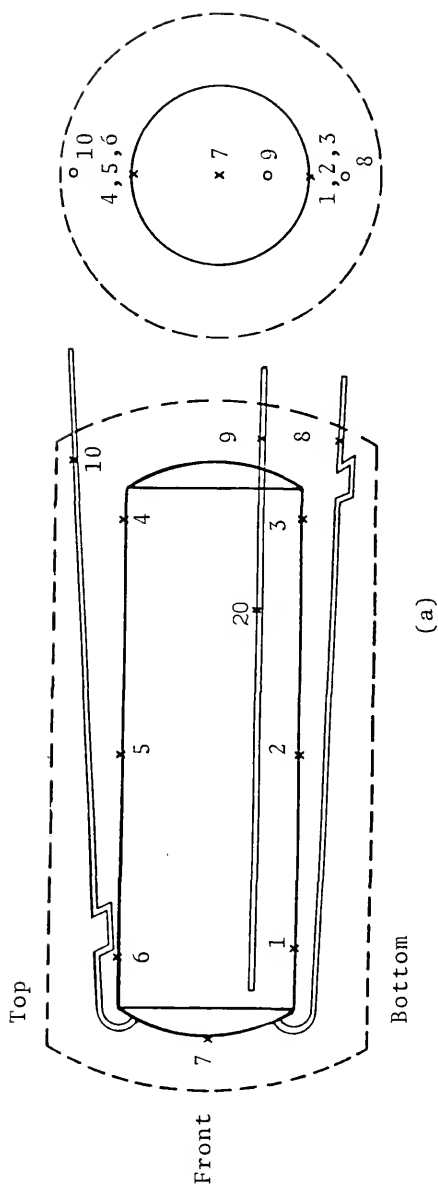
The storage tank had thermocouples attached at various points to the exterior of the inner tank, as shown in

Figure 18, and they were also placed in the powder insulation so that a temperature profile through the powder could be observed. Surface temperatures of the outer tank were taken externally.

The thermocouple port was part of the forward vacuum port. The thermocouples were fed through a u-shaped tube and the u-shaped tube was then filled with a high temperature wax. This formed an effective seal since the thermocouple port was far enough away from the heated tank so that the thermocouples were not affected by heat conduction through the wires. That is, heat did not cause the wires to expand and contract. As a result, no leaks were detected between the wire and wax seal. The thermocouples were stripped of insulation prior to emerging from the wax to prevent leaks from developing under the wire insulation.

The cylindrical portion of the inside of the outer tank was lined with a blanket of fine steel wool, grade (000). This provided the path of least flow resistance for evacuating gases from the powder insulation. It appears that the steel wool made it possible for air to flow essentially in a radial path out of the powders so that an air molecule traveled approximately 6.75 inches through the powder instead of through all of the powder from the bottom to top of the tank. It also filtered powder entrained in the evacuation flow so that only minimum filtration was needed at the

x22



Inner Tank and Outlet Ports

Figure 18

Thermocouple Location for Prototype
High Temperature Thermal Energy Storage Vessel

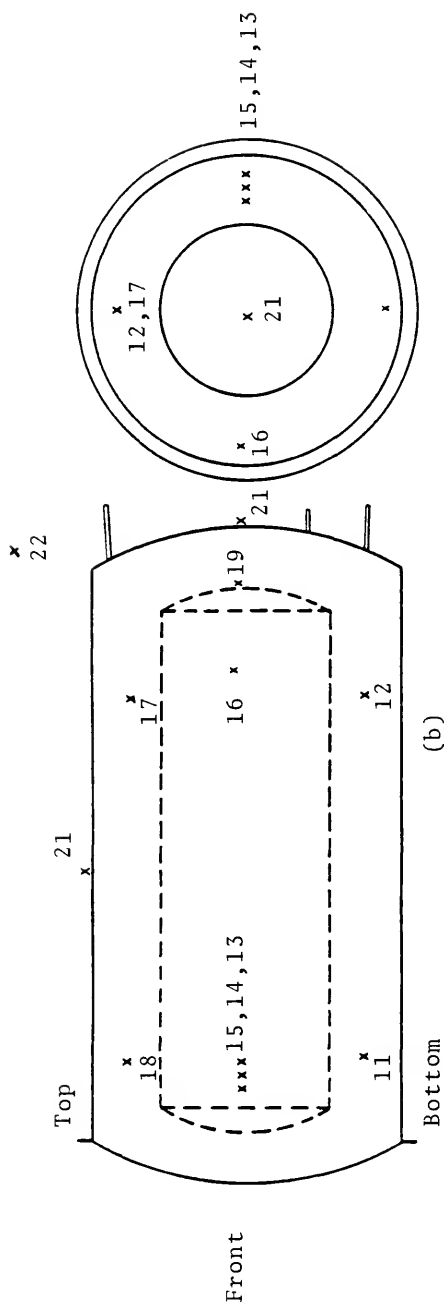


Figure 18 (Cont'd.)
 Thermocouple Location for Prototype
 High Temperature Thermal Energy Storage Vessel

inlet to the vacuum pump. The steel wool worked well because it slowed the flow of air sufficiently so that entrained particles could not be carried any great distance. This was observed in a glass cylinder that was closed at its bottom and evacuated at its top.

The steel wool blanket was fabricated by weaving the 4" wide wool strands through wire fencing. The fencing was rolled up and inserted into the outer tank where the fencing expanded, holding the steel wool against the tank surface.

The inner tank was charged with 180 pounds of vegetable oil (soybean). The powders were evacuated and the tank heater was turned on and heating of the oil was initiated. At intervals the tank was allowed to reach steady-state, so that the effectiveness of the insulation could be determined. When the oil reached a temperature near its boiling point, the power was disconnected and the tank was allowed to cool.

Results of Prototype Thermal Energy Storage System Test

A typical result of the cool down process is shown in Figure 19 for a test with the powder evacuated and a test in which the vacuum on the powder was released after the tank of oil was heated close to its boiling point ($T_{\text{boiling}} = 700^{\circ}\text{F}$ @ 1 atm. for new oil) [3].

Figure 20 shows typical temperature profiles through the evacuated powder insulation for several insulation hot face

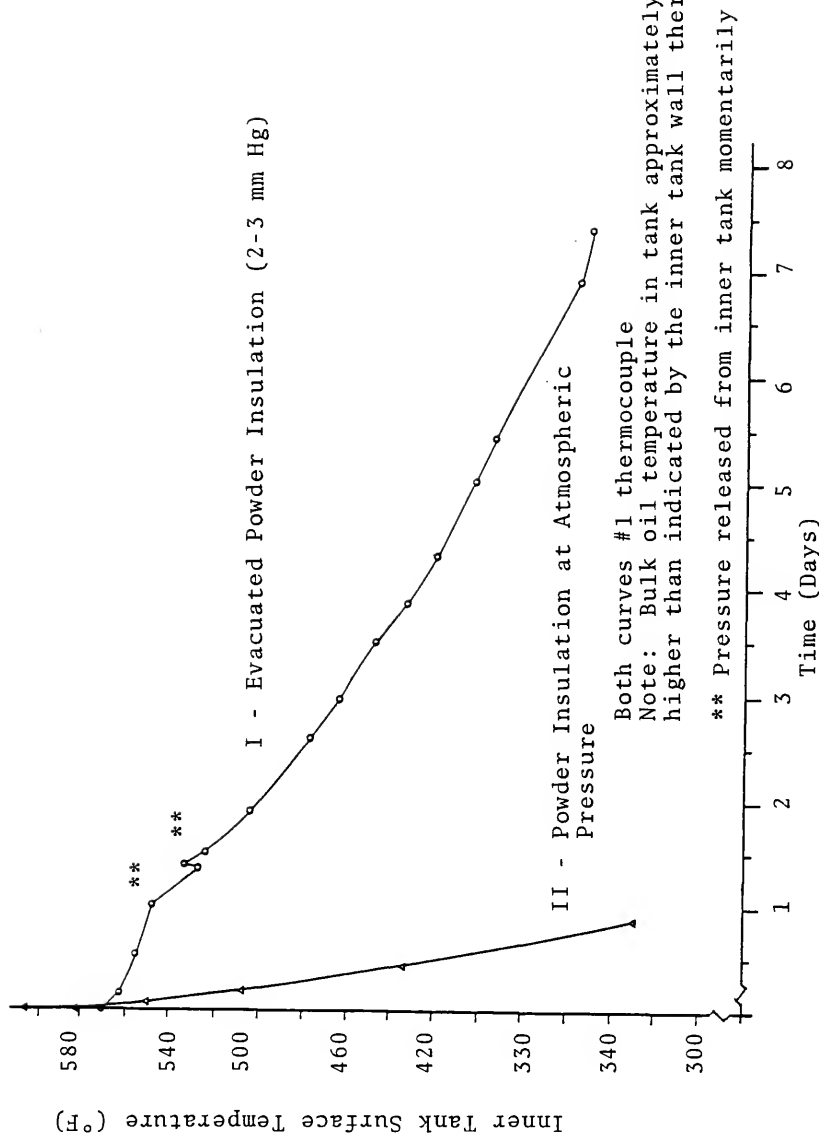


Figure 19

Cool-Down of Prototype High Temperature Thermal Energy Storage System

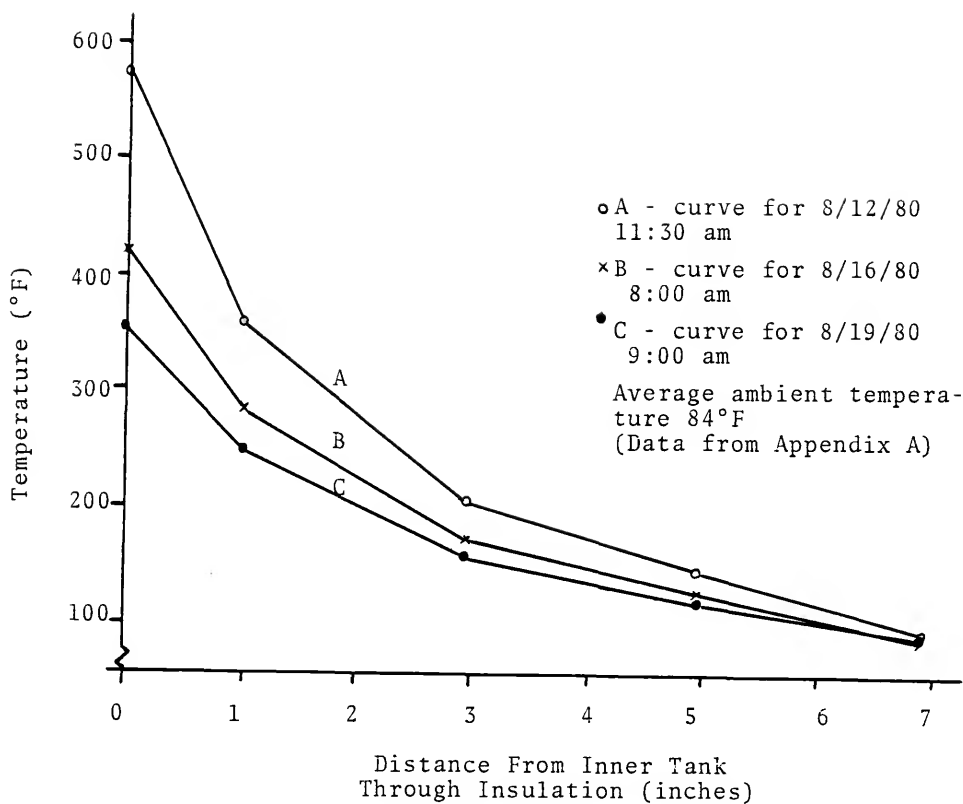


Figure 20

Temperature Profile Through
Powder Insulation Under Vacuum
(2-3 mm Hg)

temperatures. The data for Figures 19 and 20 were taken from the data presented in Appendix A.

All thermocouples were calibrated to read within $1/2^{\circ}\text{F}$ of each other when immersed at 212°F and at 70°F . When all thermocouples were fixed in place, they were checked again at room temperature to insure uniformity.

An electric resistance heater was built into the storage tank as shown in Figure 7(a). It consisted of a glass rod with a resistance heating coil wound around it and the wire was covered with a thin asbestos cover, for electrical insulation. The heater was placed in the heater port. A rheostat was used to regulate AC power to the heating element. An ammeter and a voltmeter were connected to the heating element leads to measure the power delivered to the tank. See Figure 21.

Discussion of Results for the Thermal Energy Storage System Test

Insulation performance. Figure 19 indicates that powder insulation under vacuum performed as expected as a high temperature thermal insulation. Using 70°F as the reference for the sensible energy obtainable from the storage tank, Figure 19 shows a 4.0% loss of the stored energy the first day. After one week, over 50% of the original stored energy was still available.

In contrast to the evacuated insulation, atmospheric insulation (curve II in Figure 19) lost approximately 60% of its energy in less than one day, once the vacuum was released. Specifically, in less than 18 hours, its temperature dropped to a level that took the evacuated powder insulation 168 hours (7 days) to reach.

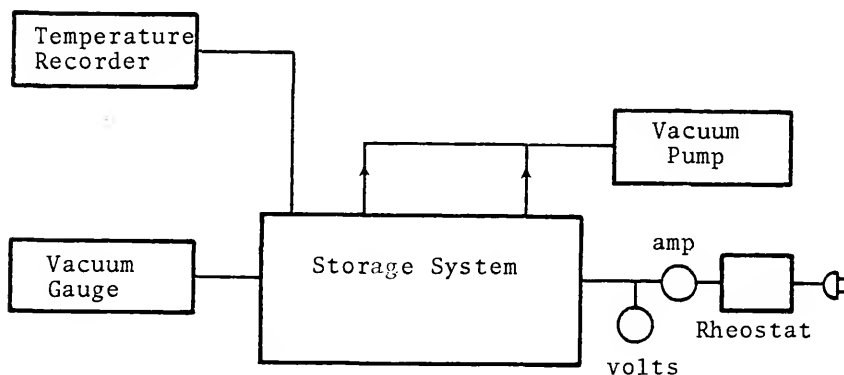


Figure 21

Storage System Test Equipment Arrangement

Figure 20 shows typical temperature profiles through the powder insulation under vacuum. The data points indicated on the graph were taken by placing thermocouples in the powder at 1, 3 and 5 inches from the hot surface boundary.

The cold face temperature was measured on the surface of the external tank. The thermocouple locations of the data points of Figure 20 are shown in Figure 18 and a reference list is shown in Appendix A.

The temperature profiles of Figure 20 raise some interesting questions concerning the reasons for the rapid increase in the slope of the curve as the hot surface temperature increases and as the hot surface boundary is approached. Several causes for this are

1. for cylindrical geometry where energy transport is radial, a decreasing temperature profile is expected since the amount of insulating material increases with an increasing radius,
2. the particle thermal conductivity may decrease with a rise in temperature,
3. the powder next to the hot surface boundary may impede radiative transfer,
4. the local effect of temperature on lowering gaseous molecular energy transfer is more pronounced near the hot surface boundary than near the cold surface boundary, and
5. an interaction between the above mechanisms may be occurring with a consequential local rise in temperature as the hot surface is approached.

The shape of Curve A in Figure 20 suggest that radiant and gaseous molecular energy transfer may be responsible for the temperature gradient next to the hot surface boundary. This is evidenced by the sudden rise in temperature of Curve A between a point three inches from the hot surface and the hot surface. Hence, although the net

effect of radiant transport through the powders may be negligible its local effect, in combination with the other modes of energy transport near the hot surface boundary is significant. The shape of the right-hand portion of Curve A, as well as Curve B and Curve C, suggest that linear heat transfer mechanisms control energy transfer in that region. Also that portion of the curves are more consistent with constant heat flux distribution through cylindrical geometry according to the term $\ln (r_o/r_i)$ in Equation 41.

The temperature profiles shown in Figure 20 indicate that powder insulation under vacuum is effective since the outer boundary temperature was only a few degrees higher than ambient.

Heating of organic oil. Curve I of Figure 19, page 106, begins at a temperature well below the normal boiling point of soybean oil, that is 700°F at atmospheric pressure. In the first run of the high temperature storage system, the oil was heated to the vicinity of its boiling point. The consequent rise in tank pressure caused tank failure. This was not anticipated as the storage system had been pressure tested to 250 psig and the air and oil vapor pressure, at an oil temperature of 700°F, was expected to be less than 75 psig. Analysis of the tank failure showed that the heater area was undersized. Since the expected natural convection coefficient of heat transfer of organic oil is small, about 7.5 Btu/hrft²°F at 670°F, the tempera-

ture of the oil next to the heater surface can reach or exceed its boiling point. This indicates that if organic oil is used for heat transfer purposes, then the heat transfer surface must be large or the temperature differences between it and the oil must be small, if the oil is to be used near its boiling temperature. This also implies that for forced convection systems, high flow rates will be required [3]. Also, if the oil is to be used near its boiling point, then safety precautions must be taken in view of the high pressures that may be encountered.

Steel wool blanket. The steel wool blanket (grade 000) performed well in suppressing powder entrainment during the evacuation of air from the powder insulating material. The operating principle of the steel wool blanket was observed by evacuating powder in a glass cylinder. As the air was evacuated, small holes formed in the powder permitting air to escape. As the air exists through the small holes, its velocity in the cavity was sufficient to entrain powder particles. When steel wool was placed over the powder surface, the air jets coming out of the powder surface were diffused by the steel wool, thus minimizing entrainment.

Overall storage vessel performance. During the heating phase of the storage vessel performance test the system was periodically allowed to attain a steady state condition. At that point the current and voltage to the

heater element were monitored and the apparent conductivity of the insulation material was approximated by the following,

$$Q_{\text{loss}} = K_a \pi \Delta T \left(\frac{2L}{\ln(r_o/r_i)} + \frac{D^2}{2\Delta X} \right) \quad (50)$$

The first part of Equation 50 represents the heat loss from the cylindrical portion of the tank and the second part represents the heat loss through the ends of the tank. The diameter of the end of the tank was approximated by taking the arithmetic mean of the inner and outer tank diameters to compensate for edge losses. Solving Equation 50 for the apparent conductivity, K_a , and evaluating with the following conditions,

$$\begin{aligned} Q_{\text{loss}} &= 200 \text{ Btu/hr} \\ r_o &= 1.25 \text{ ft (outer tank radius)} \\ r_i &= 0.67 \text{ ft (inner tank radius)} \\ L &= 4.17 \text{ ft (inner tank length)} \\ \Delta T &= (530 - 93)^\circ\text{F} \\ \Delta X &= 0.58 \text{ ft (insulation thickness)} \\ D &= 1.92 \text{ ft} \end{aligned}$$

gives,

$$K_a \sim 0.0097 \text{ Btu/hrft}^\circ\text{F}$$

This value is consistent with apparent conductivity values obtained in the conductivity test cell. It should be

recalled that the density of the powder in the storage vessel was about 32 lbm/ft³. With this density, the vacuum level was allowed to operate between 2-3 mm Hg.

Heat losses through the inlet and outlet pipes, the thermocouple wires, and the tank support cables were found to be negligible as explained in Chapter V. The heater port was found to carry about 5% of the total heat loss. If a larger heater port should be needed, as indicated earlier, then heat loss through it could become significant, and care should be taken in its design.

Tank support. The small stainless steel cable used in the high temperature thermal energy storage vessel was found to be sufficient for its intended purpose. Heat loss through the cables was found to be negligible as indicated in Chapter V.

The test data for the Tyler Sieve #500 compressed powder, Figure 16, indicates that it may be possible to let the insulating powder support the inner tank. This could be accomplished by using compressed powders under the tank and then filling the remaining volume with loose fill or uncompressed powders. The benefit of this design would be the elimination of a heat loss path and the elimination of external supports needed to support the weight of the inner tank and its heat storage medium.

Cost of high temperature storage. Inevitably, cost will be a primary factor in governing the use of the high

temperature thermal energy storage systems. Assume a self-sufficient residential system requires a storage capacity of 10^6 Btu. The required storage volume is then approximated as follows

Heat Storage Material	Volume (ft ³)	Sphere Radius (ft)
Soybean Oil (600°F)	65	2.5

The oil storage tank will require two tanks. The outer tank radius is assumed to be 0.5 feet larger than the inner tank radius. Table 8 gives an estimated cost of this storage system.

The economics of the high temperature storage vessel are greatly enhanced if the latent heat of fusion of a heat storage medium is used along with sensible heat storage. For example, if NaNO_3 [35] were used instead of organic oil, then the high temperature storage vessel would contain approximately 2.13×10^6 Btu. This gives a storage cost of \$493 - 1221 per 10^6 Btu. This phase change material requires a rather elaborate heat exchanger and it will displace some of the heat storage material. This will make the above cost higher but the cost is competitive with that of low temperature thermal energy storage vessels such as hot water storage.

Table 8
Estimated Manufacture's Cost for Storage Vessels

System Specifications

Tank volume (ft ³)	
(a) inner	65
(b) outer	113
Insulation volume (ft ³)	48
Tank material - carbon steel	-

Cost Range of Fabrication [36]

Spherical tanks (two required)	\$500 - 2000 [†]
Insulation powder (diatomaceous earth)	\$ 50 - 100*
Labor - 40 hrs @ \$10.00/hr	\$400
Tank testing - 5 hrs @ \$20/hr	\$100
Cost for storing 10 ⁶ Btu (Storage medium - soybean oil @ 600°F)	\$1050 - 2600

[†]Cost depends upon quantity, source of purchase and wall thickness of tanks.

*Cost depends upon quantity, grade of material, particle size and source of purchase.

Uncertainty in the Measurement of K_a

The uncertainty analysis is presented in Appendix C concludes that a maximum uncertainty in the physical measurements of the apparent thermal conductivity coefficient to be approximately 4.1% at a specified pressure. This value is within acceptable engineering limits for experimental work. Included in Appendix C is also a discussion concerning the methodology in the use of thermocouples for temperature measurement.

CHAPTER VI

CONCLUSIONS AND RECOMMENDATIONS

Conclusions

Based on the work described in this dissertation, the following conclusions are given.

1. The overall use of powder insulation under vacuum for high temperature thermal energy storage is technically and economically feasible.
2. Thermal conductivity values of 0.0029 - 0.110 Btu/hrft²°F were achieved experimentally for vacuum levels ranging from 0.5 - 3.0 mm Hg and hot surface temperatures ranging from 340 - 711°F.
3. A vacuum level of 0.5 mm Hg to 10 mm Hg is the recommended pressure range for operating powder insulation. The choice of vacuum level will depend upon particle size, particle material, type of gas present, temperature level, and system costs.
4. Small particles of diatomaceous earth suppress gaseous conductivity more effectively than large particles when compared using the same residual gas of the same pressure.
5. From the theoretical considerations the apparent thermal conductivity of powder under vacuum can be improved by selecting residual gases that inhibit molecular energy transport, such as gases with high molecular weight and specific heat ratios.
6. An evacuated powder can be used to support a load and still maintain a relatively low thermal conductivity.

7. The desirable characteristics of an insulating powder particle are small particle size, spherical geometry, low thermal conductivity, non-conducting electrically, non-corroding, stable at elevated temperatures, universally available, and inexpensive.
8. Particle size and distribution, as measured by mechanical separators, of the materials used in this study did not appear to be consistent with electron microscope photographs of the material. The particles as viewed by the electron microscope appear to be much smaller and of various sizes.
9. The use of a fine steel wool blanket permitted evacuation of air from the storage vessel with minimal entrainment of the powder insulation.

Recommendations

Based on the work carried out in developing this dissertation, the following recommendations are made.

1. There is need for quantitative data and correlation techniques for predicting actual particle size, shape, and distribution.
2. Methods can be explored for fabricating porous powders that will minimize heat transfer by particle-to-particle conductivity while at the same time suppressing gaseous and radiative conductivity.
3. Experimental data at low pressure and high temperature for apparent thermal conductivity of porous powders, with various interstitial gases, would be very useful.
4. The evaluation of the temperature-pressure relationship of organic oils along with an evaluation of the corrosion potential of the oils at elevated temperatures would be useful in designing high temperature thermal energy storage vessels.

5. There is a need for an investigation into the design of high temperature storage vessels for use with phase change material. The primary area of investigation would be to identify and develop suitable heat exchangers or other means of extracting energy from the solidifying phase change material.

APPENDIX A
STORAGE VESSEL TEST DATA

Thermocouple Number and Location
For Prototype Thermal Energy Storage Vessel Test

<u>Thermocouple No.*</u>	<u>Location (See Figure 18)</u>
1	Bottom, front
2	Bottom middle
3	Bottom, back Positions on
4	Top, back inner tank
5	Top, middle 1 - 7
6	Top, front
7	Center, front
8	Bottom Inlet Pipe 4-1/2" from inner tank
9	Heater Port 4-1/2" from inner tank
10	Top Inlet 4-1/4" from inner tank
11	Bottom, front 4" from inner tank
12	Bottom, back 4" from inner tank
13	Side, front 5" from inner tank
14	Side, front 3" from inner tank
15	Side, front 1" from inner tank
16	Side, back 4" from inner tank
17	Top, back 4" from inner tank
18	Top, front 4" from inner tank
19	Center, back 4" from inner tank
20	Heater Port - on outside of heater rod in heater port
21	Outer tank surface (moveable probe)
22	Ambient

* Chromel-Alumel thermocouples, referenced to ice bath.

TEST A
 Prototype Thermal Energy Storage Kerosene Test Data
 Cool Down Time for Evacuated Powder Insulation

Date	Time	1	2	3	4	5	6	7	8	9	10	11	12	13	14	15	16	17	18	19	20	21	22	Comments
7/23	8:45 pm	85 F	all points																					
7/30	11:30 am	197	195	197	198	198	195	197	174	287	128	146	113	100	117	176	105	140	116	115	294	45	-	-
	9:30 am	225	252	255	258	258	253	255	207	303	141	197	110	118	152	211	129	142	148	146	547	87	-	-
7/31	11:30 am	322	322	325	329	329	322	324	241	447	171	271	125	145	207	222	166	156	140	128	500	97	-	-
	12:00 pm	360	282	277	278	278	271	278	197	261	162	285	104	162	239	301	187	163	187	170	320	-	-	-
8/1	9:30 am	328	342	348	352	359	348	344	234	430	163	297	183	159	230	260	183	165	134	172	638	113	-	-
8/2	9:30 am	318	345	349	365	362	346	347	237	312	267	350	174	194	282	239	231	220	162	180	515	132	-	-
8/3	10:30 am	239	350	353	360	360	352	352	239	315	273	369	175	204	290	236	241	223	162	100	531	170	-	-
	11:45 pm	411	426	413	429	437	416	433		344	282	389	179	213	305	304	250	235	168	202	573	175	-	-
8/4	8:30 am	413	431	431	429	436	424	442	267	364	304	422	260	236	326	274	267	263	180	212	600	178	-	-
8/4	10:30 pm	386	502	514	497	514	482	504	335	435	292	434	189	210	333	335	262	250	237	215	509	100	-	-
8/5	9:30 am	321	437	431	436	436	426	439	301	365	252	397	178	197	305	266	235	204	226	198	400	101	-	-
8/6	9:00 am	319	328	340	332	325	330	344	293	307	302	302	150	162	237	240	187	162	180	103	380	95	-	-
8/7	8:45 am	338	348	360	352	352	347	349	255	310	147	227	109	140	189	253	140	117	132	127	404	97	-	-
	4:00 am	302	407	418	417	417	408	400	286	365	134	223	104	134	181	284	132	112	126	126	568	95	-	-
	9:00 pm	321	415	447	450	448	441	447	300	347	140	241	107	138	189	239	135	124	130	127	376	98	-	-
11:45 pm	421	416	443	419	421	418	417	-	330	170	286	134	154	224	288	164	167	163	142	351	-	-	-	

TEST A, Continued

Date	Time	1	2	3	4	5	6	7	8	9	10	11	12	13	14	15	16	17	18	19	20	21	22	Comments
8/8	8:45 am	459	455	491	456	458	457	454	-	371	141	234	106	137	191	303	132	126	131	123	-	93	-	
	11:30 am	497	490	496	493	495	494	489	-	440	140	237	107	137	191	300	133	136	131	127	604	95	-	
	3:30	533	535	535	528	530	529	531	-	413	145	245	113	141	195	370	137	274	137	130	-	-	-	
	8:45	535	536	537	530	533	532	534	-	412	149	249	113	141	196	372	137	302	137	128	-	-	-	
	9:45	532	533	533	528	531	530	532	-	409	149	248	109	138	194	370	133	304	133	123	-	98	-	
	11:40	532	535	535	528	531	530	532	-	408	149	247	107	137	193	375	131	250	132	120	-	93	-	
8/9	12:30 pm	527	528	527	524	526	525	527	-	403	147	245	104	134	192	340	129	182	128	119	-	93	-	
	7:30 am	508	510	508	506	506	507	507	-	381	147	238	102	132	186	329	126	153	124	114	-	80	-	
	9:00 am	503	503	502	501	502	502	502	-	377	145	235	99	130	185	323	124	137	122	112	-	80	-	
	12:30 pm	506	506	505	505	505	506	504	-	390	150	239	105	136	189	328	130	144	127	121	-	95	-	
	6:30 pm	503	503	502	501	503	502	500	-	389	152	240	108	139	191	329	133	150	130	126	-	102	-	
	8:45 pm	500	500	500	499	499	501	500	500	-	387	152	239	107	137	190	325	132	137	129	122	-	95	-
	11:00 pm	499	499	498	498	499	499	496	-	386	150	236	113	135	189	323	128	125	127	120	-	91	-	

TEST A

Date	Time	1	2	3	4	5	6	7	8	9	10	11	12	13	14	15	16	17	18	19	20	21	22	Comments
8/10	7:30 am	496	487	497	497	498	498	495	-	385	143	230	109	133	185	322	126	120	125	117	-	89	-	
	11:30 am	509	506	505	508	508	508	503	-	405	142	230	110	134	185	327	127	120	125	120	-	93	-	power 487.5 watts
	3:30 pm	519	516	516	518	519	519	514	-	413	144	233	115	136	187	335	131	139	128	126	-	102	-	
	8:00 pm	550	543	543	549	550	549	540	-	455	141	235	112	134	187	347	138	140	126	124	574	93	88	
	11:30 pm	513	572	573	582	583	582	572	-	482	139	239	110	132	188	359	126	139	125	122	624	85	80	
8/11	1:00 am	594	585	585	592	593	592	584	-	479	139	240	111	133	189	364	127	144	126	123	598	88	81	power 53 watts
	2:00 am	592	587	586	591	592	591	586	-	431	140	243	113	135	191	361	128	130	127	122	-	89	85	pressure of inner oil tank vented
	3:30 am	599	600	599	597	598	597	597	-	439	144	114	135	192	599	410	129	272	131	120	-	89	85	
	1:00 pm	586	586	586	585	585	585	585	-	440	150	257	119	140	198	380	134	228	133	124	-	96	91	
	3:45 pm	582	583	582	580	582	581	581	-	438	152	258	121	143	200	375	136	220	134	131	-	98	95	power 780 watts
8/12	1:30 am	574	573	573	573	573	573	571	-	432	153	259	120	142	201	355	135	143	133	124	-	91	87	
	5:30 am	572	572	571	572	573	572	570	-	433	152	259	119	142	201	358	134	143	133	124	-	88	83	
	8:30 am	571	569	569	570	571	570	569	-	430	148	258	117	141	201	357	133	164	133	124	-	91	85	
	*11:30 am	573	571	571	572	573	572	569	-	432	147	258	117	142	202	355	134	150	133	124	-	89	83	power 96.3 watts
	3:00 pm	565	564	563	565	565	564	562	-	418	148	259	121	144	203	354	137	153	137	124	-	92	89	*power off - cool off begins
	6:30 pm	557	557	556	557	557	557	555	-	413	147	259	120	143	203	349	137	150	136	126	-	95	91	

*Cool down begins.

TEST A, Continued

Date	Time	1	2	3	4	5	6	7	8	9	10	11	12	13	14	15	16	17	18	19	20	21	22	Comments
8/13	11:00 pm	548	547	548	549	548	548	546	-	407	144	257	118	142	202	344	134	146	134	124	608	91	84	
	8:00 am	528	528	528	528	528	528	527	-	394	139	255	115	139	201	334	132	139	133	122	589	86	80	
	9:30 am	534	535	534	535	535	534	534	-	402	138	256	160	139	201	342	133	139	133	124	587	-	-	
	11:15 am	524	524	524	524	524	524	524	-	393	138	256	136	141	202	334	134	141	134	126	583	91	86	
	10:00 pm	563	563	562	563	563	563	563	-	374	137	240	116	137	166	322	130	114	130	120	559	88	82	
8/14	2:30 pm	478	477	477	477	477	477	477	-	360	137	233	117	136	189	302	130	116	129	120	531	91	87	
	11:00 pm	404	404	404	404	404	404	404	-	357	134	326	119	132	184	305	127	114	124	118	516	86	74	
8/15	1:15 am	363	402	432	402	402	402	402	-	355	134	225	115	132	184	303	127	113	124	117	516	87	84	
	12:30 pm	446	446	446	446	446	446	446	-	345	130	216	111	130	177	286	125	110	121	117	497	89	86	
8/16	9:45 pm	434	434	433	434	435	434	433	-	338	131	212	111	130	176	291	125	111	121	116	483	91	82	
	8:00 am	421	421	420	420	421	420	420	-	329	127	204	105	124	169	283	120	103	116	111	470	84	80	
8/17	12:25 am	403	403	402	403	404	402	405	-	319	128	198	108	126	167	276	122	106	117	115	450	90	88	
	10:25 am	395	395	395	395	396	395	395	-	315	127	195	107	125	165	274	121	105	117	115	441	90	87	
8/18	10:15 pm	359	359	359	360	359	359	359	-	290	123	181	103	121	155	254	117	102	112	109	401	88	81	
8/19	9:00 am	351	351	350	351	351	351	351	-	285	118	175	100	117	151	250	114	99	109	108	392	86	84	
8/20	10:25 am	332	332	331	332	332	332	332	-	274	119	169	100	117	147	242	114	100	108	108	371	90	88	

TEST B

Prototype Thermal Energy Storage Vessel Test Data
Cool Down Time for Non-Evacuated Powder Insulation

Date	Time	1	2	3	4	5	6	7	8	9	10	11	12	13	14	15	16	17	18	19	20	21	22	Comments
8/22	10:30 pm	110	110	110	110	110	110	110	-	114	102	108	97	100	106	105	102	98	98	101	193	90	83	powder evacuated
8/23	5:45 am	102	102	102	102	102	102	102	-	104	81	86	77	81	85	95	82	77	78	78	108	74	74	1-2 mm lg.
	9:30 am	136	134	134	134	134	134	134	-	140	93	100	89	94	98	121	85	89	90	92	305	87	84	
	12:30 pm	146	144	145	145	145	145	145	-	148	92	100	89	94	98	129	95	90	90	94	317	90	88	
	3:30 pm	156	154	155	155	155	155	155	-	157	93	101	90	96	93	137	95	94	90	95	324	93	92	
	9:00 pm	179	177	177	177	177	177	177	-	186	93	101	90	95	98	152	94	92	90	95	427	92	80	
	11:00 pm	194	191	192	192	194	194	192	-	190	92	101	80	94	98	181	94	90	90	95	436	-	-	
8/24	10:00 am	244	242	243	244	244	277	241	-	215	91	103	87	93	98	191	91	80	87	93	460	86	83	
	4:30 pm	285	281	282	284	284	284	280	-	267	95	108	92	97	102	218	95	90	90	100	550	95	94	
	11:20 pm	326	321	322	325	325	325	320	-	297	99	112	100	98	104	239	96	99	90	99	589	93	88	
8/25	9:00 am	318	314	314	314	314	314	309	-	273	97	115	91	95	104	231	93	94	88	90	613	83	80	
	10:30 pm	407	402	403	406	406	405	400	-	419	104	128	97	100	111	281	97	101	93	104	660	90	86	powder in - 281.3 J watts
	11:45 pm	416	410	411	414	414	413	409	-	425	105	130	98	102	113	285	98	102	94	105	668	89	86	
8/26	9:00 am	411	408	409	409	400	405	408	-	342	106	137	96	102	116	279	96	100	94	97	673	85	83	
	2:30 pm	432	428	428	430	430	429	428	-	432	107	140	100	104	118	293	97	194	95	106	677	94	90	powder in - 59.12 watts
	10:30 pm	435	430	462	463	464	463	459	-	223	110	146	101	105	122	307	105	105	105	106	691	88	83	

Date	Time	1	2	3	4	5	6	7	8	9	10	11	12	13	14	15	16	17	18	19	20	21	22	Comments
8/27	8:00 am	502	501	502	409	500	499	500	-	424	111	154	101	104	125	320	90	102	96	99	652	85	82	pressure of inner tank - 20 psig
	10:50 am	530	528	525	525	525	527	-	-	441	112	161	108	106	120	383	90	106	98	101	681	87	83	pressure of inner tank - 60 psig
	*1:30 pm	604	601	603	595	595	597	602	-	450	129	176	121	108	137	-	104	354	109	111	644	-	87	vacuum on insulation released
	2:10 pm	583	582	583	569	563	565	570	-	431	165	256	123	115	172	459	138	-	-	-	-	-	92	-
	3:10 pm	551	555	557	541	542	541	551	-	413	217	335	146	133	208	393	152	351	173	148	608	114	93	-
	6:00 pm	507	504	506	506	503	500	504	-	386	254	365	173	168	256	349	202	239	212	178	560	114	94	top outlet pipe - 140°F, heater
	8:20 pm	473	468	468	468	469	469	461	-	364	250	368	187	181	273	321	214	227	224	180	522	100	91	outlet pipe - 118°F
	10:20 pm	451	448	448	440	448	446	446	-	352	243	365	182	187	278	308	217	209	225	184	490	105	90	hot spot on back end of tank - 110°F
	11:40 pm	434	429	432	424	431	429	426	-	341	238	360	187	188	279	309	217	204	255	194	481	112	88	-
8/28	8:45 am	352	348	350	342	348	347	349	-	288	205	311	167	178	252	255	195	175	201	174	391	103	87	pressure of inner tank - 44 psig
	12:00 pm	330	328	330	322	327	326	328	-	275	196	294	163	171	239	245	187	170	192	168	368	106	82	pressure of inner tank - 32 psig
	11:00 pm	263	263	264	258	262	261	263	-	229	169	239	214	152	201	208	163	150	165	148	292	102	85	-

*Vacuum on insulating powders released at this time. Cooling process.

APPENDIX B

CONVECTION HEAT TRANSFER ANALYSIS
FOR A POROUS POWDER

In powder with particle dimensions less than 0.2 inches in diameter, investigators, such as Hill and Wilhelm [20], found no evidence of convective heat transfer in quiescent gas-solid beds. The condition encountered in their study was similar to those of this work.

The above investigation applied particularly to a gas-solid bed at atmospheric pressure. This study was primarily interested in heat transfer through powders under vacuum conditions. Hence, for the conditions mentioned above, it was concluded that convective heat transfer would be eliminated. Justification for this conclusion follows.

Convective heat transfer in the laminar region can be expressed in the following form,

$$Nu = \left(\frac{hb}{k_f} \right) = G(Ra)^{\frac{1}{4}} \quad (51)$$

where b is a characteristic dimension of a given geometry, G is a constant of the order of unity and Ra is the Rayleigh number. In expanded form Equation 51 can be written as,

$$Nu = G(g\beta C_p \rho^2 b^3 \Delta T / \mu k_f)^{\frac{1}{4}} \quad (52)$$

The term β for a perfect gas is $\beta = 1/T$. The task now is to show that convective heat transfer is negligible for conditions encountered in this study. Specifically, one

must show that convective heat transfer is negligible over the temperature and pressure range encountered. These values are 250-1000°F and 0.5-760 mm Hg.

If Equation 52 is evaluated at the 250°F and 1000°F at a pressure of one atmosphere, for $b = 0.015$ ft, $\Delta T = 10^\circ\text{F}^+$, the Nusselt number is found to be of the order of unity for both temperatures. Since the Nusselt number is given by Equation 2, then

$$\text{Nu} = \frac{hb}{k} \sim 1 \quad (2)$$

and the convective heat transfer coefficient is seen to be of the same order of magnitude as the thermal conductance of the fluid. That is,

$$h \sim k/b \quad (53)$$

A decrease in the heat transfer coefficient with a decrease in pressure, as calculated by Equation 52, is illustrated by substituting for the density term,

$$\rho = P/RT \quad (7)$$

⁺ Assumed maximum temperature difference between particles or between particles and a container boundary.

This substitution, along with setting $\beta = 1/T$, gives

$$\text{Nu} = G(gC_p P^2 b^3 \Delta T / \mu_f k_f R^2 T^2)^{1/4} \quad (52)$$

Restricting the above equation to a continuum, it is clear that the Nusselt number and, hence, the convective heat transfer coefficient decreases as the pressure decreases. The decrease is proportional to $P^{1/2}$. More importantly, the above equation shows that the Nusselt number is proportional to $(P/T)^{1/2}$. Typically, the operating conditions encountered in this study were that pressure, P , would be decreased and temperature, T , would increase. Assuming a continuum exists in a gas-solid bed for a fluid at 1 mm Hg, and temperature increased from 250°F (710°R) to 1000°F (1460°R), the Nusselt number, and hence the convective heat transfer coefficient, would decrease by approximately two orders of magnitude, as compared to values obtained at atmospheric conditions. The above factors indicate that convective heat transfer is no longer significant at reduced pressures and high temperatures.

The above paragraph illustrates that convective heat transfer becomes negligible as the pressure changes from 760 mm Hg to 1 mm Hg. In the region of 1 mm Hg and where the gas molecules are confined such that $\text{Kn} > 1$, the assumption of a continuum no longer applies. In this case, convec-

tion heat transfer is negligible and molecular thermal conductivity of the fluid is proportional to pressure. This situation has been explored in Chapter III.

APPENDIX C
UNCERTAINTY IN THE MEASUREMENT OF K_a

The uncertainty analysis presented here deals with the uncertainty in the physical measurement of the apparent thermal conductivity coefficient, K_a . The apparent thermal conductivity coefficient, as given by Equation 42, is a function of

$$K_a = K_a(E, I, \theta, r_o, r_i, L, T_H, T_C) \quad (54)$$

Equation 54 does not explicitly contain the variable pressure, P , under which the insulating material was tested. Hence, the uncertainty in the measurement of K_a will be given with K_a as the dependent variable and pressure, P , as the independent variable.

Before proceeding to calculate uncertainty in the measurement of K_a , an explanation of the difficulty of including pressure as an explicit variable in the analysis is in order. If K_a in Equation 41 is replaced with the sum of Equations 19 and 37

$$K_a = \frac{9\gamma-5}{4(\gamma-1)} \left(\frac{2R_u}{\pi M T} \right)^{1/2} (1/P\bar{D} + 1/B)^{-1} + \frac{C n \pi K_s D_c N_A}{2 N_h \ln (D_c/y^*)} \quad (55)$$

then variables are introduced whose values are not readily available, such as k_s , \bar{D} , n , N_A , N_h , D_c . Using this approach would require assuming values for these parameters and this would negate the purpose of calculating uncertainty.

The standard deviation, ΔK_a , in the measurement of K_a is calculated with [37]

$$\Delta K_a = \left(\sum_i^j \left(\frac{\partial K_a}{\partial z_i} \right)^2 u_{zi}^2 \right)^{1/2} \quad (56)$$

where

z = independent variable

u_{zi} = instrument deviation in measuring z .

Equation 55 is based on the assumption that the standard deviation of the input parameter, z , is Gaussian in nature.

Applying Equation 56 to Equation 42,

$$K_a = \frac{EI \ln(r_o/r_i)}{2\pi L (T_H - T_C)} \quad (42)$$

and dividing the result by K_a yields

$$\begin{aligned} \frac{\Delta K_a}{K_a} = & \left[\left(\frac{u_E}{E} \right)^2 + \left(\frac{u_I}{I} \right)^2 + \left(\frac{-u_{r_o}}{r_o \ln(r_o/r_i)} \right)^2 \right. \\ & \left. + \left(\frac{u_{r_i}}{r_i \ln(r_o/r_i)} \right)^2 + 2 \left(\frac{u_{T_H}}{T_H - T_L} \right)^2 + \left(\frac{-u_L}{L} \right)^2 \right]^{1/2} \quad (57) \end{aligned}$$

The maximum deviation of each of the instruments used in the measurement of the parameters in Equation 54 and for the pressure measurement is given below.

<u>Parameter</u>	<u>Instrument</u>	<u>Maximum Division</u>
Temperature	Chromel-Alumel thermocouple	$\pm 0.75\%$
Current	Ammeter-Westinghouse Type PA-4	$\pm 2.5\%$
Potential	Weston-Schlumberger Digital VOM	$\pm 1.0\%$
Length	Stainless Steel Scale	$\pm 1.3 \times 10^{-3}$ ft.
Pressure	McLeod Vacuum Gauge	$\pm 3.0\%$

Two sample problems to illustrate the range of uncertainty will be calculated for typical conditions, at both high and low temperatures, encountered in the measurement of the apparent thermal conductivity coefficient

Sample 1.

$$K_a = 0.0072 \text{ Btu/hrft}^\circ\text{F (Table 5, line 5)}$$

$$T_H = 730^\circ\text{F (Table 5, line 5)}$$

$$T_C = 104^\circ\text{F (Table 5, line 5)}$$

$$E = 25.0\text{V}$$

$$I = 0.55 \text{ amperes}$$

$$L = 1.0 \text{ ft}$$

$$r_o = 0.163 \text{ ft}$$

$$r_i = 0.089 \text{ ft}$$

Applying these parameters and the instrument deviations from the above list into Equation 57 yields

$$\begin{aligned}
\frac{\Delta K_a}{K_a} &= \left[\left(\frac{0.01 \times 25.0}{25.0} \right)^2 + \left(\frac{0.025 \times 0.55}{0.55} \right)^2 + \left(\frac{0.0013}{0.163 \times 0.605} \right)^2 \right. \\
&\quad + \left(\frac{0.0013}{0.089 \times 0.605} \right)^2 + 2 \left(\frac{0.0075 \times 730}{730 - 104} \right)^2 \\
&\quad \left. + \left(\frac{0.0013}{1} \right)^2 \right]^{\frac{1}{2}} \\
\frac{\Delta K_a}{K_a} &= 0.041
\end{aligned}$$

That is $\Delta K_a = \pm 4.1\%$ of K_a @ $P = 1000$ mm Hg $\pm 3\%$. Note that in the numerator of the first three terms in the above sample calculation that the instrument deviation, given as a percentage of the scale reading, was multiplied by the scaled value to obtain the instrument deviation.

Sample 2

$$K_a = 0.00407 \text{ Btu/hrft}^\circ\text{F (Table 5, line 8)}$$

$$T_H = 452^\circ\text{F (Table 5, line 8)}$$

$$T_C = 87^\circ\text{F (Table 5, line 8)}$$

$$E = 11.3 \text{ V}$$

$$I = 0.4 \text{ amperes}$$

$$L, r_o, r_i - \text{same as above}$$

Calculating as before, one obtains

$$\frac{\Delta K_a}{K_a} = 0.041$$

or, $\Delta K_a = \pm 4.1\% @ K_a @ P = 1000 \text{ } \mu\text{m Hg} \pm 3\%$.

From the above calculations it is apparent that deviations in the measurement of K_a fall within an acceptable range.

Of the variables measured for calculating K_a , the variable temperature requires additional comments concerning methodology in the use of the temperature transducers or thermocouples. All thermocouples junctions were welded together to form a small bead. The thermocouples used to measure T_H were brazed to a copper surface and all excess brazing material was removed. The asbestos-covered lead wires from the junction were placed adjacent to the copper surface to minimize conduction losses from the thermocouple junction. The thermocouple used to measure T_C was welded together and the resulting beaded junction was ground away until a thin, flat junction was obtained. This junction was covered with a small piece of ceramic insulation and then held against a surface for temperature measurement. Efforts were made to maintain constant pressure on the temperature probe when a surface temperature was taken. This procedure yields more consistent data [38].

The cold junction of the thermocouple was an ice bath. Even though ordinary tap water was used in the bath, a high quality mercury-in-glass thermometer showed negligible deviation from 32°F.

BIBLIOGRAPHY

1. Farber, E. A., Morrison, C. A., Ingley, H. A., "A Residential Solar Cooking System," 11th Annual Intersociety Energy Conservation Conference, September, 1976.
2. Cope, N. A., Ingley, H. A., Farber, E. A., Morrison, C. A., "Dynamic Response Analysis of a Solar Powered Heliotropic Fluid-Mechanical Drive System," 2nd Miami International Conference on Alternative Energy Sources, December 10-13, 1979.
3. Ingley, Herbert A., Vegetable Oils: Liquid Coolants for Solar Heating and Cooling Applications, prepared by the Solar Energy and Energy Conversion Laboratory, University of Florida, Gainesville, Florida for the Department of Energy, Contract No. EM-78-C-04-4298, 1980
4. Wark, Kenneth, Thermodynamics, 2nd Edition, McGraw-Hill, New York, 1971.
5. Angrist, Stanley W., Direct Energy Conversion, 3rd Edition, Allyn and Bacon, Incorporated, Boston, Massachusetts, 1976, p. 50.
6. Jakob, Max, Heat Transfer, John Wiley & Sons, Incorporated, New York, 1950, pp. 83-91.
7. Strong, H. M., Bundy, F. P., Bovenkerk, H. P., "Flat Panel Vacuum Thermal Insulation," Journal of Applied Physics, Vol. 31, No. 1, January 1969, p. 41.
8. Smoluchowski, M., Proceedings of the 2nd Refrigeration Congress, Vol. 2, 1910, pp. 187-193.
9. Kistler, S. S., and Caldwell, A. G., Industrial Engineering Chemistry, Vol. 26, 1934, p. 658.
10. Wilkes, Gordon B. Heat Insulation, John Wiley & Sons, Incorporated, New York, 1950, p. 95.
11. Peterson, P., The Heat-Tight Vessel, University of Lund, Sweden (1951), Office of Naval Intelligence, Translation No. 1147, 1953.

12. Klett, Robert D., Analytical Thermal Design of Cellular Insulation and Laminated Composites, Sandia Laboratories, Albuquerque, New Mexico, SAND 74-0232.
13. Delil, A. A. M., and Heemskerk, J. F., "A Theoretical Investigation of Gas Conduction Effects on Multi-Layer Insulation Performance," Netherlands Agency for Aerospace Programs, NIVR Nr 1766, 1976.
14. Niendorf, L. R., The Design, Development and Delivery of High Temperature Insulation Systems for SNAP-21 Thermoelectric Power Systems, Union Carbide Corporation, Linde Division, Tonawanda, New York, June 1970.
15. Black, A., Fowle, A. A., Glaser, P.E., Development of High Efficiency Insulation, Author D. Little, Incorporated, Cambridge, Massachusetts.
16. Sparrow, E. M., Gupta, B. P., Wehner, G. K., Research Applied to Solar-Thermal Power Systems, NTIS Report: NSF/RANN/SE/GI 34871/PR/75/2.
17. Chubb, Talbot A., "Energy Storage Tank," E. O. Hulburt Center for Space Research, Naval Research Laboratory, Washington, D.C., June 1976.
18. Baumeister, Theodore, and Marks, Lionel S., Editors, Standard Handbook for Mechanical Engineers, 7th Edition, McGraw-Hill, New York, 1967, pp. 4-94.
19. Johns-Manville, Insulation Product Information, A.I.A. File No. 37-D.
20. Hill-F. B., and Wilhelm, R. H., "Radiative and Conductive Heat Transfer in a Quiescent Gas-Solid Bed of Particles: Theory and Experiment," American Institute of Chemical Engineers, Vol. 5, December 1959, p. 486.
21. Kennard, E. H., Kinetic Theory of Gases, McGraw-Hill, Inc., New York, 1938.
22. Klett, Robert D., Analytical Thermal Design of Cellular Insulation and Laminated Composites, Sandia Laboratories, Albuquerque, New Mexico, SAND 74-0232, p. 12.
23. Haung, Francis F., Engineering Thermodynamics, Macmillan Publishing Company, Incorporated, New York, 1976, p. 138.
24. Dushman, S., Scientific Foundations of Vacuum Technique, John Wiley, & Sons, Incorporated, New York, 1949, p. 32.

25. Knudsen, Martin, Kinetic Theory of Gases, John Wiley & Sons, Incorporated, New York, 1950, pp. 46-51.
26. Dushman, S., Scientific Foundations of Vacuum Technique, John Wiley & Sons, Incorporated, New York, 1949, p. 49.
27. Arpaci, Vedat S., Conduction Heat Transfer, Addison-Wesley Publishing Company, Reading, Massachusetts, 1966, p. 104.
28. Shigley, Joseph E., Mechanical Engineering Design, McGraw-Hill, New York, 1977, p. 75.
29. Argo, W.B., and Smith, J.M., "Heat Transfer in Packed Beds," Chemical Engineering Progress, Vol. 49, No. 8, August 1953, pp. 443-451.
30. Schotte, William, "Thermal Conductivity of Packed Beds," American Institute of Chemical Engineers, Vol. 6, No. 1, March 1980, pp. 63-67.
31. Damkoehler, G., "Der Chemie Ingenieur," Euken Jacob, Vol. 3, Part 1, Adndemische Verlagegesellschaft M.B.H., Leipzig, 1937.
32. Brownell, Lloyd E., and Young, Edwin H. Process Equipment Design, John Wiley & Sons, Incorporated, New York, 1959, pp. 141-154.
33. Baumeister, Theodore, Editor, Standard Handbook for Mechanical Engineers, McGraw-Hill, New York, 7th Edition, 1967, pp. 4-94.
34. American Society of Heating, Refrigerating and Air Conditioning Engineers, Incorporated, Handbook of Fundamentals, George Banta Co. Inc., Menasha, Wisconsin, 1972, p. 273.
35. Masayuki Kamimoto, Tadayoshi Tanaka, Tatsuo Tani, and Takashi Horigome, "Investigation of Nitrate Salts for Solar Latent Heat Storage," Solar Energy Journal, Vol. 24, No. 6, 1980, pp. 581-587.
36. Private Communication with Mr. Jack Nilsson, Seige Corporation, Easley, S.C., September, 1981.
37. Holman, Jack Phillip, Experimental Methods for Engineers, 3rd Edition, McGraw-Hill, New York, 1978.
38. Honig, Daniel A., Requirements of a Thermocouple Probe Which Gives a Reproducible Means of Determining Surface Temperature, High Honors Project, University of Florida, 1957.

EXTENDED BIBLIOGRAPHY

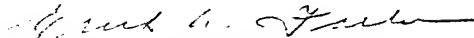
- Chen, John C., and Churchill, Stuart W., "Radiant Heat Transfer in Packed Beds," American Institute of Chemical Engineers Journal, Vol. 9, No. 1, 1963, p. 35-41.
- Ho, C. Y., and Taylor, R. E. (editors), Thermal Conductivity, Proceedings of the Eighth Conference, Plenum Press, New York, 1969, pp. 897-911.
- Larkin, Bert K., and Churchill, Stuart W., "Heat Transfer by Radiation through Porous Insulation," American Institute of Chemical Engineers Journal, Vol. 5, No. 4, 1959, pp. 467-474.
- Masamune, Shinobu, and Smith, J. M., "Thermal Conductivity of Porous Catalyst Pellets," Journal of Chemical and Engineering Data, Vol. 8, No. 1, 1963, pp. 54-58.
- Smith, W. R., and Wilkes, G. B., "Thermal Conductivity of Carbon Black," Industrial and Engineering Chemistry, Vol. 36, No. 12, pp. 1111-1112.
- Reynolds, C. D., and Ardany, Z. L., Palarite Thermal Insulation, Union Carbide Corporation, Oak Ridge Y-12 Plant, Oak Ridge, Tennessee, TID-4500, April, 1970.
- Touloukian, Y. S., Thermophysical Properties of Matter, Vol. 2, IFI/Plenum, New York, 1970.
- Whetley, S. J., and Mallett, A. J., Foam Plastic Insulation for High Temperature and Shock Protection, Union Carbide Corporation, Nuclear Division, Oak Ridge Gaseous Diffusion Plant, Oak Ridge, Tennessee, 1968.
- Yagi, Sakoe and Kunnii, Daizo, "Studies on Effective Thermal Conductivities in Packed Beds," American Institute of Chemical Engineers Journal, Vol. 3, No. 3, pp. 373-380.

BIOGRAPHICAL SKETCH

Norman Alan Cope was born May 11, 1947, in Gaston County, North Carolina. He graduated from Stanley High School in June, 1965. He attended Gaston Community College from 1965 to 1967 and the University of North Carolina at Chapel Hill from 1967 to 1969. From the latter he received a degree in American history. After graduation from the University of North Carolina at Chapel Hill, he received basic training in the North Carolina Army National Guard. Work on a bachelor's degree in mechanical engineering was begun at the University of North Carolina at Charlotte in 1971 and completed in 1975. In 1972 he married Elizabeth Ann Brown. Two sons, Christopher Alan and Eric Keith, were born in November 1973, and November 1977, respectively. Work on his Master of Engineering degree in mechanical engineering began in 1975 and was completed in 1977. Work on the degree of Doctor of Philosophy was begun in 1977.


Norman Alan Cope is a member of American Society of Mechanical Engineers, the American Society of Heating, Refrigerating and Air Conditioning Engineers and the American Section of the International Society of Solar Engineering.

I certify that I have read this study and that in my opinion it conforms to acceptable standards of scholarly presentation and is fully adequate, in scope and quality, as a dissertation for the degree of Doctor of Philosophy.



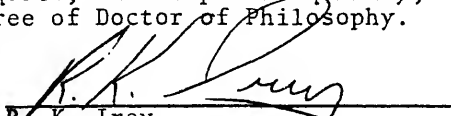
Erich A. Farber, Chairman
Professor of Mechanical
Engineering

I certify that I have read this study and that in my opinion it conforms to acceptable standards of scholarly presentation and is fully adequate, in scope and quality, as a dissertation for the degree of Doctor of Philosophy.



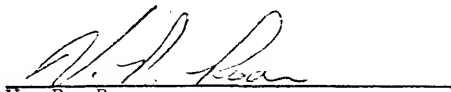
H. A. Ingley
Associate Professor of
Mechanical Engineering

I certify that I have read this study and that in my opinion it conforms to acceptable standards of scholarly presentation and is fully adequate, in scope and quality, as a dissertation for the degree of Doctor of Philosophy.



R. K. Ireby
Professor of Mechanical
Engineering

I certify that I have read this study and that in my opinion it conforms to acceptable standards of scholarly presentation and is fully adequate, in scope and quality, as a dissertation for the degree of Doctor of Philosophy.



V. P. Roan
Professor of Mechanical
Engineering

I certify that I have read this study and that in my opinion it conforms to acceptable standards of scholarly presentation and is fully adequate, in scope and quality, as a dissertation for the degree of Doctor of Philosophy.

T. T. Bowman

T. T. Bowman
Associate Professor of
Mathematics

This dissertation was submitted to the Graduate Faculty of the College of Engineering and to the Graduate Council, and was accepted as partial fulfillment of the requirements for the degree of Doctor of Philosophy.

December 1981

Hubert A. Blevins

Dean, College of Engineering

Dean for Graduate Studies and
Research

UNIVERSITY OF FLORIDA



3 1262 08553 1860